# The influence of astrocytes and their culturing environment on blood-brain barrier modeling in a microfluidic chip

Michaela Hällevall

2017


LUND
UNIVERSITY

Master's Thesis in

Biomedical Engineering

Lund Univeristy, Faculty of Engineering LTH
Department of Biomedical Engineering
*In collaboration with University of Twente*
*BIOS Lab on a Chip group*

Examiner: Maria Tenje
Supervisors: Marinke van der Helm and Anette Wolff

# Abstract

The blood-brain barrier (BBB) is a highly selective barrier separating the brain from the circulatory system. The physical barrier is built up by a monolayer of endothelial cells, which is the main component used for *in vitro* modeling. To create more physiologically relevant *in vitro* models, the field of organs-on-chips has recently been introduced, combining microfluidics and microengineering to create culture environments for cells. To mimic the BBB, a continuous monolayer of brain endothelial cells is cultured inside these organ-on-chip devices. A step towards more *in vivo* like models is the introduction of co-cultured astrocytes, a brain-specific cell type in close contact with the blood-brain barrier *in vivo*. Astrocytes are reported to have a function in inducing and maintaining BBB-specific properties of the endothelial cells. During injury to the brain, astrocytes become reactive, changing their function, morphology and molecular expression. *In vitro* it has been shown that the state of astrocytes is influenced by their culture environment. In this study, a method to incorporate hydrogels seeded with astrocytes in a microfluidic channel is presented, along with an investigation on the effect of different hydrogel compositions on astrocyte reactivity and morphology. Firstly, using a silane-based surface treatment a collagen type I hydrogel seeded with astrocytes was successfully incorporated and fixated in a microfluidic channel inside a polydimethylsiloxane device. Secondly, by varying collagen type I and hyaluronic acid concentrations, the lowest astrocyte reactivity was found in the hydrogels containing only collagen type I and in a mixed gel of collagen type I and hyaluronic acid with a low total gel concentration. A mixture of collagen type I and hyaluronic acid resulted in the most star-shaped astrocytes, characteristic morphology for astrocytes *in vivo*. Because of the small sample size, further investigation is recommended before conclusions can be drawn on the best hydrogel composition. The results from these two experiments were used to establish a co-culture system in a blood-brain barrier-chip. Unfortunately, as no continuous monolayer of endothelial cells was formed inside the chip and air bubbles inside the hydrogel structures affected the astrocyte culture, the effect of the presence of astrocytes cultured in a three dimensional environment could not be quantified. In order to achieve a reliable co-culture system optimization of chip design and protocol for incorporation of hydrogel is recommended.

# Preface

This master thesis was carried out within the BIOS Lab on a Chip group at the University of Twente, in collaboration with the department of Biomedical Engineering at Lund University. The project was started on the 7th of February and finished on the 30th of August and it was supervised by Marinke van der Helm from the University of Twente and Anette Wolff from Lund University.

**Acknowledgements**

For all the help with supervising me I would like to give a special thanks to Marinke van der Helm, Loes Segerink, Andries van der Meer and Anette Wolff. It is your guidance, advice and support that has helped me through these six months. In excess of these I would also like to thank Martijn Tibbe and Joshua Loessberg-Zahl for all their help, both with practical dilemmas in the lab as well as with good ideas and discussions. Finally, I would like to say a big thank you to everyone in the BIOS group for the good time I have had in Enschede.

# Abbrevations

| | |
|---|---|
| AC | Alternating current |
| AM | Astrocyte medium |
| AJs | Adherens junctions |
| APTES | (3-aminopropyl) triethoxysilane |
| BBB | Blood-brain barrier |
| BioMEMS | Biomedical microelectromechanical systems |
| CNS | Central nervous system |
| DAPI | 4’,6-diamidino-2-phenylindole |
| DC | Direct current |
| ECM | Extracellular matrix |
| EGM-2 | Endothelial cell growth medium |
| FITC | Fluorescein isothiocyanate |
| GA | Glutaraldehyde |
| GFAP | Glial fibrillary acidic protein |
| GFP | Green fluorescent protein |
| HA | Hyaluronic acid |
| hCMEC/D3 | Human cerebral microvascular endothelial cells |
| HEMA | 2-hydroxyethyl methacrylate |
| JAMs | Junctional adhesion molecules |
| NVU | Neurovascular unit |
| PBS | Phosphate-buffered saline |
| PDMS | Polydimethylsiloxane |
| PEG | Poly(ethylene glycol) |
| PEGDA | Poly(ethylene glycol) diacrylate |
| PLL | Poly-L-lysine |
| PVA | Polyvinyl alcohol |
| RF | Radio frequency |
| RFP | Red fluorescent protein |
| TEER | Transendothelial electrical resistance |
| TJs | Tight junctions |
| UV | Ultraviolet |
| VE-cadherin | Vascular endothelial cadherin |
| ZO | Zonula occludens |
| 2D | 2 dimensional |
| 3D | 3 dimensional |

# Table of Contents

# 1 Introduction

The BBB is a highly selective physical barrier between the circulatory system and the brain. The substances that are able to cross this barrier are highly controlled by specialized endothelial cells in order to maintain the environment needed for the brain tissue [1]. However, this makes it problematic to develop drugs able to cross the barrier and reach the brain. Today, the most commonly used method for testing the effects of new drugs is through animal testing, also usually referred to as *in vivo* tests. *In vivo* models enable testing in the natural and very complex environment of an organ. Nevertheless, next to ethical concerns, there are several drawbacks of animal testing. The most important one is the large number of drugs that fail in a late stage of development after having shown promising results in animal tests, either due to poorly designed preclinical trials or difference in response between animals and humans [2]. Other testing methods are *in vitro* studies where the tests are carried out in cell cultures, either in a 2 dimensional (2D) or 3 dimensional (3D) environment. One example of a commonly used model for BBB research is the culturing of cells in the commercially available Transwell. The Transwell consists of two compartments separated by a porous membrane on which cells can be cultured. One of the problems with this model is that it is usually too simplified and is not able to incorporate natural physical parameters found *in vivo*, such as blood flow [3]. Therefore a new field of *in vitro* models has been introduced, which is called organs-on-chips. The concept of organs-on-chips is to combine microfluidics and bioengineering in an effort to faithfully replicate the smallest structure that builds up an organ, by culturing cells in a dynamic environment [4].

Up to this date, there are several research groups working on developing a BBB-on-chip [5–7]. The different models that have been published differ in design, material and cell lines being used, although they are all trying to replicate the basic structure of the BBB, which consists of brain endothelial cells [8]. In some models endothelial cells are co-cultured with other brain-specific cells, in an attempt to make the model more physiologically relevant, as some of these cells are capable of increasing the BBB-specific properties of the endothelial cells [9-10]. A lot of focus has especially been put on a brain-specific cell type called astrocytes, which has the ability to induce BBB-specific properties in the endothelial cells [11]. Astrocyte function and morphology are dependent on the culturing method. When cultured in common plastic dishes the cells exhibit a state found during damage to the brain defined as reactive astrocytes, while

cultured in an environment better resembling the *in vivo* situation, for example in hydrogels, they adapt the non-reactive state found in healthy brain [12].

## 1.1 Aim and outline

The aim of this master thesis project is to culture astrocytes within a hydrogel mimicking the healthy 3D brain environment and evaluate their effect on BBB-function when co-cultured with brain endothelial cells inside a microfluidic chip.

To achieve this aim, three different experiments were carried out, where the goals of the experiments are to

1. Functionalize the surface of the material used for the microfluidic chip, in order to ensure the attachment between hydrogel and channel walls.

2. Seed astrocytes inside different hydrogel compositions and evaluate morphology and reactivity.

3. Co-culture endothelial cells and astrocytes within a hydrogel in a BBB-chip and evaluate the effect on the barrier by measuring the barrier function.

The results of the two first experiments are applied to the third and final experiment.

In this report the BBB biology and different laboratory models mimicking the BBB are explained in more detail, followed by some relevant background information about the methods and materials used for the experiments performed. Afterwards, the three different experiments will be described in separate chapters containing methods, results and a short discussion about the used method and obtained results. As some of the methods are the same for all three experiments, these have been put in the appendix for easy reference. In the last part a general discussion is presented followed by conclusions and suggestions for future work.

# 2 Blood-brain barrier

The BBB is the physical barrier that separates the brain from the body's circulatory system. The purpose of the BBB is to create a highly controlled and selective barrier in order to maintain the specific homeostasis of the central nervous system (CNS), protecting the brain tissue [13]. The reason why this extra protection is important for the brain is the limited regenerative capability of brain tissue, as neurons in most cases are not capable of dividing once fully differentiated. Therefore, the BBB has a strict control of the transport of molecules such as ions, neurotransmitters, macromolecules, neurotoxins and nutrition that can cause harm to the cells of the brain [14]. The main structure building up the BBB is a monolayer of endothelial cells, which is also a component of the neurovascular unit (NVU). The NVU maintains and controls the environment of the brain and it consists of several different cell types, the extracellular matrix (ECM) of the brain and a special ECM for the endothelial cells called the basement membrane. The different constituents of the NVU influence the function and structure of the BBB, both in health and disease [15].

Modeling the BBB is of great importance for drug development and toxicology tests and the two most established models up to date are *in vivo* tests, carried out in animal models, and *in vitro* tests in Transwell models [16]. The disadvantages of these models have led to a need for new and more reliable ones, and within the field of organs-on-chips researchers are trying to create models capable of meeting these needs. The main idea is to incorporate microchannels in materials such as glass or polydimethylsiloxane (PDMS) where cell cultures, either grown directly on the material of the channel or incorporated in hydrogels, are exposed to a fluidic flow [17]. For evaluation of the cell barrier in *in vitro* models of the BBB there are two commonly used measurement methods: permeability tests and resistance measurements carried out across the cell layer, referred to as transendothelial electrical resistance (TEER) measurements [18].

## 2.1 Neurovascular unit

The NVU consists of endothelial cells that form the BBB, a basement membrane, pericytes, astrocytes, neurons, microglia and the ECM of the brain [15]. A full overview of the NVU and its components can be seen in Figure 1. The main function of the NVU is to control the exchange of fluids and molecules between the brain and the blood in order to maintain an optimal environment for the brain. This is achieved by controlling the permeability across the barrier [19]. It is worth

noting that it is still unclear exactly how each of the components contribute to the specific properties of the BBB [13].

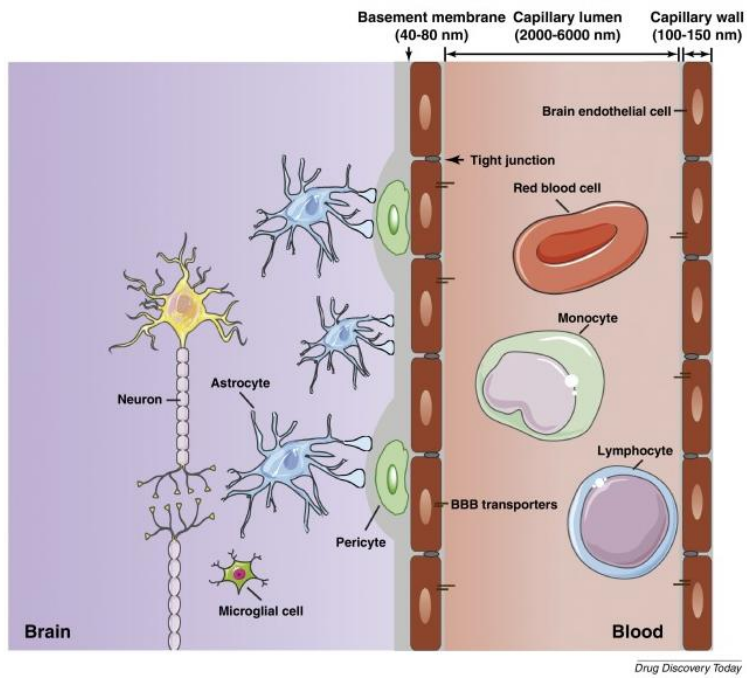


**Figure 1.** A schematic of the NVU. Embedded in the ECM of the brain neurons, astrocytes, microglial cells and pericytes are present while endothelial cells, lined with the basement membrane, make up the barrier separating brain and blood. Reprinted from [20].

### *2.1.1 Endothelial cells*

The main component that contributes to the specific properties of the BBB is cerebral endothelial cells. These cells are ordered in a monolayer and together with the basement membrane they create the wall of the capillaries, which makes them the main physical barrier between the brain and the circulatory system [11]. Endothelial cells line blood vessels in all organs, allowing them to control the exchange of substrates between the blood and the organ [21]. The main difference between brain endothelial cell-layers and endothelial cell-layers in other parts of the body is that the connections between the cerebral endothelial cells are typically 50-100 times tighter. This leads to a lower degree of transport between the cells (paracellular transport), meaning that the main way of transport between the blood and the brain is through well-regulated transcellular transport [11,15]. These tight connections between cells are established by two main groups of protein complexes called tight junctions (TJs) and adherens junctions (AJs). In addition, the cerebral endothelial cells have more BBB-specific properties that

contribute to the selective barrier that differs from other endothelium. Some of these properties are the absence of fenestrae (small pores in endothelial cells that allow for rapid molecular exchange), a low pinocytotic activity (uptake of extracellular fluid into the cell by endocytosis) and a high concentration of mitochondria, meaning that the cells can have a higher metabolic activity [22]. The specific properties of the endothelial cells and the high concentration of tight junctions lead to the highly controlled transcellular and paracellular transport, causing the transport pathways across the barrier to be limited to only specific molecules and compounds. In Figure 2 the different transport pathways across the barrier are shown. The degree of permeability across the BBB depends on the integrity of the barrier. Tighter connected endothelial cells will cause less compounds to cross the cell layer via the paracellular pathway [14].

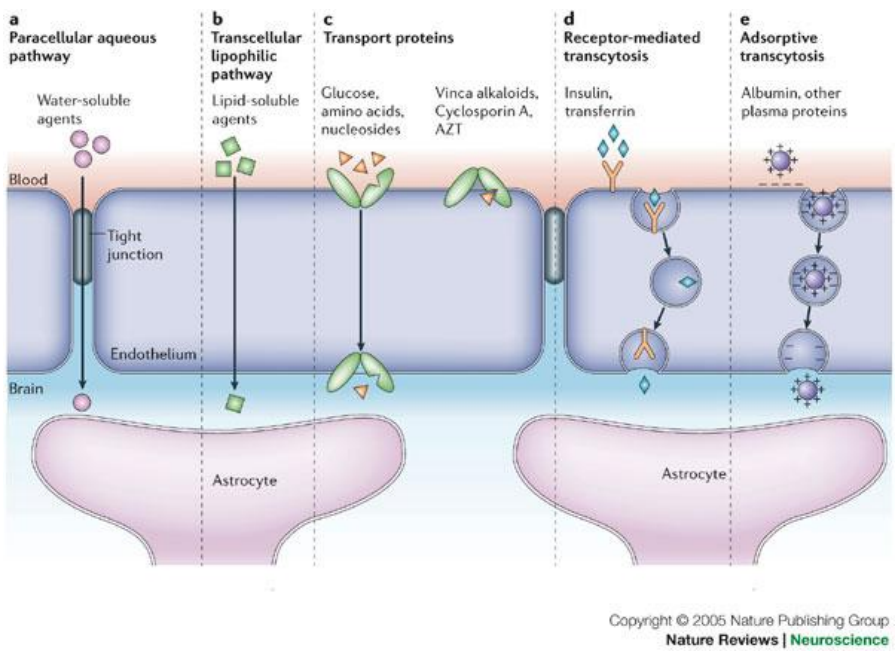


**Figure 2.** The different transport pathways across the BBB. In pathway **a** water-soluble agents are capable of crossing through paracellular pathways, while in pathways **b**-**e** transport is through transcellular pathways. In **b** lipid-soluble agents are capable of crossing the cell membrane through the transcellular lipophilic pathway. In **c** transport proteins will transfer compounds such as glucose and amino acids across the cell barrier. In **d** and **e** transport across the endothelial cells is carried out through transcytosis, either receptor-mediated (**d**) or through adsorption (**e**). Reprinted from [1].

### *Tight junctions*

One of the main contributors to the strong connection between the endothelial cells within the BBB are TJs. The TJs are built up by three main groups of transmembrane molecules connecting the endothelial cells. The two groups responsible for cell-cell interaction are called occludins and claudins, while the third group, called junctional adhesion molecules (JAMs), is responsible for organizing the structure of the TJs. All protein groups and their positions in the cell membrane can be seen in Figure 3. Occludin and claudin proteins are connected to the cytoskeleton of the cells through zonula occludens (ZO) proteins, a group of proteins positioned in the cytoplasm of the cell close to the membrane [23]. Occludin was the first tight junction protein to be discovered, although experiments with occludin-deficient mice showed no distinct difference in BBB function compared to wild-type mice [24]. These results indicate that occludin is not necessary for the formation of the TJs, but instead may act as an extra support structure [15]. The second protein group is the claudin family, and these proteins are reported to give rise to the specific characteristics of the barrier tightness and restricted paracellular diffusion [23]. In experiments with claudin-5-deficient mice it was shown that the size-selectivity for smaller molecules across the barrier decreased, indicating the importance of these proteins when it comes to the permeability of the barrier [25]. The third family of proteins present at the TJs, JAMs, are thought to have a role in organizing the structure of the TJs as well as controlling the movements of immune cells across the barrier [23]. The degree of TJs present between the cells will have a large influence on the tightness of the barrier: the more TJs present, the tighter the connection between the cells [26].

### *Adherens junctions*

The AJs are positioned just basal to the tight junctions (see Figure 3). The main AJ protein is a transmembrane protein called vascular endothelial cadherin (VE-cadherin) that together with another group of proteins called catenins forms complexes that provide cell attachment and structural integrity between the endothelial cells. Due to this, the presence of AJs is important for the formation of TJs [14].

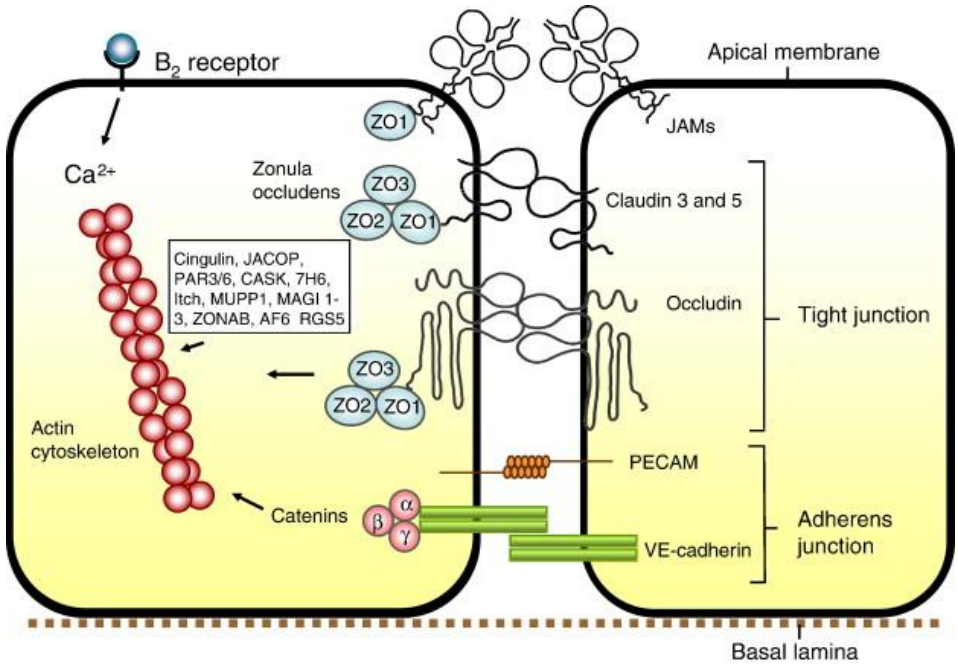


**Figure 3.** An illustration of the connections between endothelial cells. The TJs make up the main connection between the cells and consist of three types of transmembrane molecules: occludins, claudins and JAMs. These are connected to actin filaments via ZO proteins. The AJs are positioned basal to the TJs. Reprinted from [14]

### *2.1.2 Basement membrane*

The basement membrane is a 50 - 100 nm thick layer of specialized ECM, which can be found close to monolayers of cells, such as endothelium and epithelium, separating them from the surrounding tissue. The main components of the basement membrane are collagen type IV, laminin, perlecan and nidogen. In addition there are several other minor components present with varying concentrations depending on the organ [27]. Within the NVU the basement membrane is situated between the endothelial cells and the astrocytic endfeet, providing stability for the cells and controlling cell processes and signaling between cells with its ECM components [28].

### *2.1.3 Pericytes*

Pericytes are embedded within the basement membrane and enclose part of the surface of the cerebral endothelial cells through cytoplasmic extensions. The pericytes are reported to have an important role when it comes to blood vessel stabilization, angiogenesis (formation of new blood vessels), blood flow regulation and maintenance of BBB properties [29]. Pericytes are capable of

affecting the BBB properties by altering the permeability over the barrier and the integrity of the TJs [15].

### *2.1.4 Astrocytes*

Astrocytes are a cell type specific for the CNS and they are situated in close contact with neurons and blood vessels within the CNS. Some of the known functions of astrocytes are providing physical support, taking up and excreting compounds from and to endothelial cells and neurons, maintaining homeostasis of the brain and inducing BBB specific characteristics of the endothelial cells [30]. Astrocytes have a spherical cell body with long and thin processes, resulting in a star-shaped morphology, that are connected to neurons and endothelial cells through their endfeet. These connections are of great importance for uptake and excretion of molecules between the cells. For example at the contact points with blood vessels astrocytes take up glucose and water and transfer these to neurons, and through neuron-controlled signaling they excrete molecules regulating dilation and contraction of the vessels. Another function is to induce BBB properties in endothelial cells, although it is still unclear how this is achieved [30].

During damage to the CNS astrocytes respond by changing from a non-reactive state to a reactive state. The reactive state is characterized by an increased cell volume as well as an increase in the number of cells. It has been shown that during the reactive state astrocytes upregulate their expression of several molecules such as growth factors, cytokines, enzymes and intermediate filaments, such as glial fibrillary acidic protein (GFAP) [31]. Depending on the damage, the presence of different agents will trigger an activation of the astrocytes. In Figure 4 agents that trigger an activation of astrocytes are shown as well as the cause for their presence.

One of the most common markers used for identifying astrocytes from other cell types is GFAP, mainly present in astrocytes. GFAP is a part of the cytoskeleton of the astrocytes and the main function is to define and maintain the star-shape that is typical for astrocytes [32]. While low levels of GFAP are expressed in most astrocytes during their non-reactive state, there is an upregulation of GFAP expression when reactive [31].

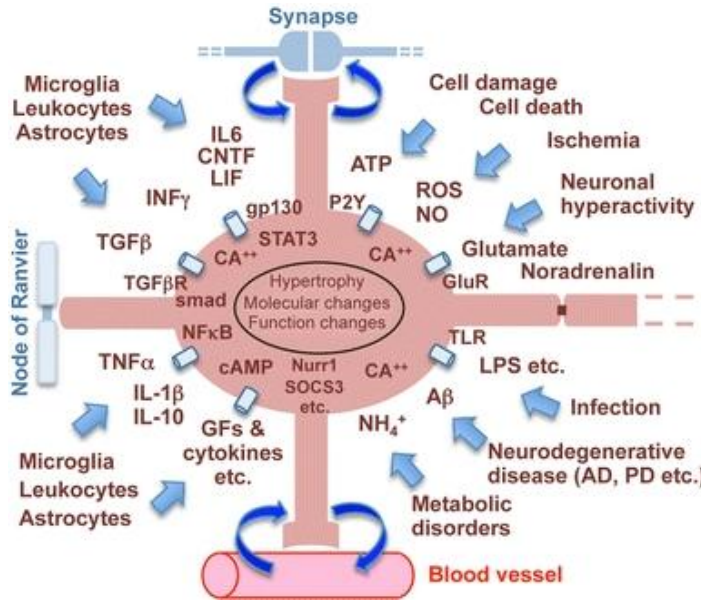


**Figure 4.** A schematic of molecular interactions with an astrocyte. Agents related to brain injuries will trigger the activation of astrocytes, leading to hypertrophy, molecular changes and functional changes of the cell. Reprinted from [30].

### *2.1.5 Neurons*

Neurons can either be directly connected to blood vessels or indirectly via astrocytes [33]. The role of neurons for the BBB properties is still not fully understood, although it is thought that they regulate some functions of the barrier [13]. One example of this is that neurons are capable of influencing the blood flow in order to meet their metabolic needs. This mechanism is referred to as neurovascular coupling, and through neurotransmitter-based signaling neurons can either directly or indirectly, in that case through astrocytes, regulate the cerebral blood flow [34].

### *2.1.6 Microglia*

Microglial cells are situated within the CNS and function as an immune defense for the brain. The microglia can either be in a resting or activated state and will have different morphology depending on the state. In the resting state, which occurs in healthy brain tissue, the cell has a small body with long and thin processes, which it uses to survey the tissue for potential threats. In the activated state the long processes are lost and a shape similar to phagocytes, an important cell for the immune response, is adopted. This state occurs in the presence of pathology to the CNS [35-36]. There are several studies indicating that during the active state of the microglia cells they excrete inflammatory factors causing disruption of the BBB, associated with neurodegenerative diseases such as Alzheimer's disease [37].

### *2.1.7 Extracellular matrix of the brain*

The ECM of the brain differs in its composition when compared to the ECM of other tissues. The common ECM components in the rest of the body, such as collagen and fibronectin, are only present in very low concentrations in the brain ECM [38]. Instead, the ECM of the brain has been shown to mainly contain compounds such as proteoglycans, containing binding sites for the polysaccharide hyaluronic acid (HA), and the ECM protein tenascin [39]. Due to the high density of cells within the brain tissue, only about 20% of the total brain volume is extracellular space, meaning that the degree of ECM in the brain is very low compared to other tissues [40].

## 2.2 BBB modeling

For a better understanding of neurovascular diseases and the effects of new drugs on the BBB, reliable models for testing are needed. The mainly used models for BBB research are *in vivo* and *in vitro* models. Two examples of *in vitro* models used for BBB research are the Transwell setup and BBB-on-chip. As the cells in *in vitro* BBB-models are not exposed to their natural environment there is a need for measurement methods to evaluate the reliability of these models as well as to measure the experimental conditions investigated. For BBB-models the main focus is on the integrity of the barrier, and the two most commonly used methods to evaluate the barrier is through permeability tests and TEER measurements.

### *2.2.1* In vivo *models*

The method that gives the best results for testing effects of drugs and to get a better understanding of diseases are studies performed directly in humans. However, for ethical reasons this is not a possibility. Therefore most *in vivo* tests for new drugs are carried out in animal models [2]. The main advantage of using animal models is that it is possible to study the BBB in its natural environment. However, the numerous disadvantages such as slow and costly experiments and their ethically questionable character has lead to a search for other methods [41]. Furthermore, there are several examples of poor translation between the results obtained in animals compared to humans, causing a lot of new drugs to fail in a late stage of development. This can be the result of poorly designed and executed studies as well as the fact that animal models are not able to completely predict the human response as there are differences when it comes to molecular and metabolic pathways between species [42-43].

### *2.2.2* In vitro *models*

The *in vitro* models are based on biological components such as cells and microorganisms that have been taken out of their natural environment. The most established *in vitro* model for BBB research is a static 2D monolayer model, where a commonly used setup is the Transwell. However, there are new models being developed in order to meet the short-comings of the Transwell. One such example is the BBB-on-chip, where the cells are exposed to a dynamic environment [44].

#### *Transwell*

One of the most commonly used setups for *in vitro* modeling of the BBB is the Transwell. The Transwell consists of a well with a removable insert containing a porous membrane on which cells can be grown [45]. The membrane is typically 10 µm thick and can be made of different materials such as polycarbonate or polystyrene [2]. This model allows for mono-, co- and tri-culturing of cell types in each well, and easy handling makes it possible to perform high-throughput assays in this system [46]. A commonly used co-culturing model contains endothelial cells on the luminal side of the membrane and astrocytes on the abluminal side, and the setup can be seen in Figure 5 [47]. Even though this model is sufficient for some studies, for other studies it can be too simplified in order to be a reliable model. Another dilemma is that the environment that the cells are grown in is static [46]. *In vivo,* endothelial cells in the brain capillaries are exposed to shear

stresses between 0.3-2 Pa, which trigger responses from the cells, affecting barrier integrity and permeability across it [8,48].

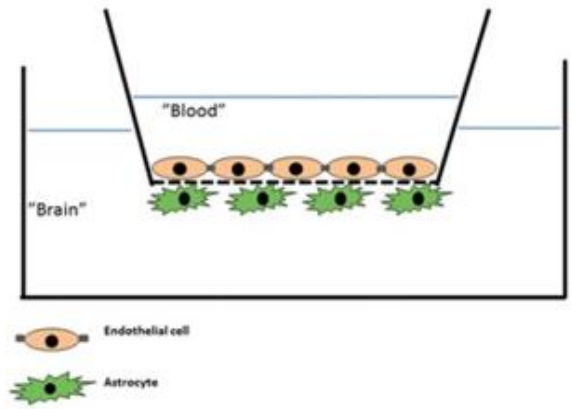


**Figure 5.** An example of a co-culture system in a Transwell model. Endothelial cells are cultured on the porous membrane on the inside of the insert while astrocytes are grown on the outside of the insert. Reprinted from [49].

### *Organs-on-chips*

Organs-on-chip is a research field where microengineering, cell culturing and microfluidics are combined in order to create a new *in vitro* model for research. Some of the drawbacks with the currently used *in vitro* models based on 2D or 3D cell culturing are the difficulties to adapt the microenvironment for the cells and to implement different physical parameters, such as compression and shear stress [50]. With the use of microfluidics and microengineering in organs-on-chips models, these problems have been addressed. Up to date several different chips for several different organs have been developed, such as lung-on-a-chip [51], gut-on-a-chip [52] and BBB-on-a-chip [7]. An example of a BBB-on-chip is shown in Figure 6.

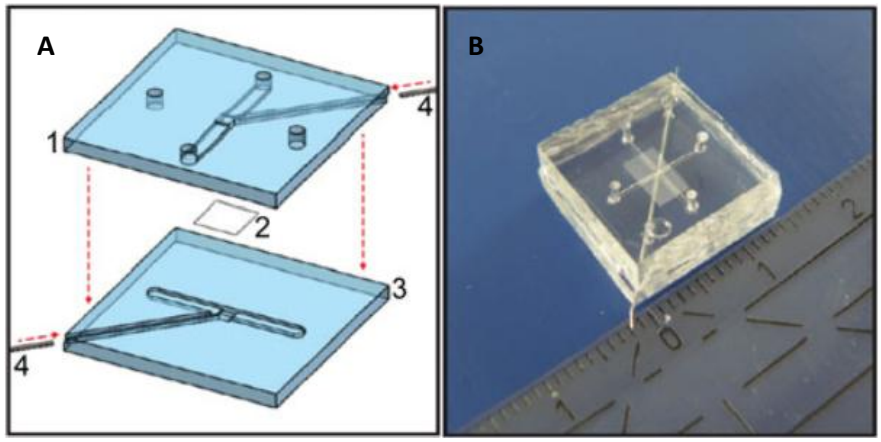


**Figure 6.** An example of a BBB-chip. In **A** a schematic of the design is showed, where **1** is the top part of the chip with a channel and holes for the inlets and outlets of the channels. **2** is the membrane separating the two channels and **3** is the bottom part of the chip with a channel oriented perpendicular to the top channel. **4** shows two electrodes connected to each of the channels. In **B** an image of the assembled chip is shown. Reprinted from [53].

In the BBB-on-chip models, a monolayer of endothelial cells is cultured under flow. In some models the endothelial cells are co-cultured with other cells from the NVU such as astrocytes, pericytes or neurons [8].

### *2.2.3 Transendothelial electrical resistance measurement*

A commonly used method for assessing the tightness of a cell layer is by measuring the electrical resistance across a cell barrier grown on a semipermeable membrane, where the resistance across endothelial or epithelial cell layers is referred to as TEER. The method is based on measuring the resistance of the barrier to charged ions or molecules across the barrier. A higher measured resistance means that there is a lower amount of charged compounds capable of crossing the barrier [54]. The electrical resistance across the pial arteries (blood vessels covering the surface of the brain) *in vivo* has been measured to lie between 1500-2000 $\Omega$ cm$^2$, compared to 3-33 $\Omega$ cm$^2$ for similar endothelia in other tissues [55].

TEER measurement is a non-invasive method allowing measurements of the integrity of the barrier in real-time with the use of electrodes [15]. During a TEER measurement the transcellular and paracellular ion flux over the cell barrier is measured. The resistance of the barrier is either characterized by the direct current (DC) or single frequency alternating current (AC) method, or through impedance spectroscopy. During impedance spectroscopy an AC signal is applied over a

frequency span and the amplitude and phase shift of the recorded current are measured [54].

To calculate the resistance from a DC or single frequency AC measurement Ohm's law is applied. With an applied voltage *V* (in V) on two electrodes positioned on each side of the barrier, the resulting current *I* (in A) is measured and the resistance *R* (in Ω) can be calculated according to equation 1.

$$R = \frac{V}{I} \tag{1}$$

To extract the TEER value a blank measurement of the membrane that the cells are to be grown on is carried out ($R_{Blank}$). The resistance of the membrane will be subtracted from the resistance obtained from the measurements on the monolayer grown on the membrane ($R_{Total}$) [54]. The resulting resistance $R_{CellLayer}$ is inversely proportional to the area of the monolayer ($A_{Memb}$) and in order to normalize the TEER to Ωcm$^2$, resistance is multiplied with area [56]. The full calculations are shown in equations 2 and 3.

$$R_{CellLayer} = R_{Total} - R_{Blank} \propto \frac{1}{A_{Memb}} \tag{2}$$

$$TEER = R_{CellLayer} * A_{Memb} \tag{3}$$

For an impedance measurement the full system consisting of the cell barrier, electrodes and culture medium is modeled as an electrical circuit. Within this model the paracellular pathway, influenced by TJs between cells, are modeled as a resistor (TEER) and the transcellular pathway across the cells are modeled as a parallel circuit of a capacitor and a resistor, representing the cell membrane. In the measurements culture medium and electrodes will also have an effect on the read-out, and the medium can be modeled as a resistor and the electrode-medium interface as a capacitor [57]. A schematic of the representative electrical circuit can be seen in Figure 7.

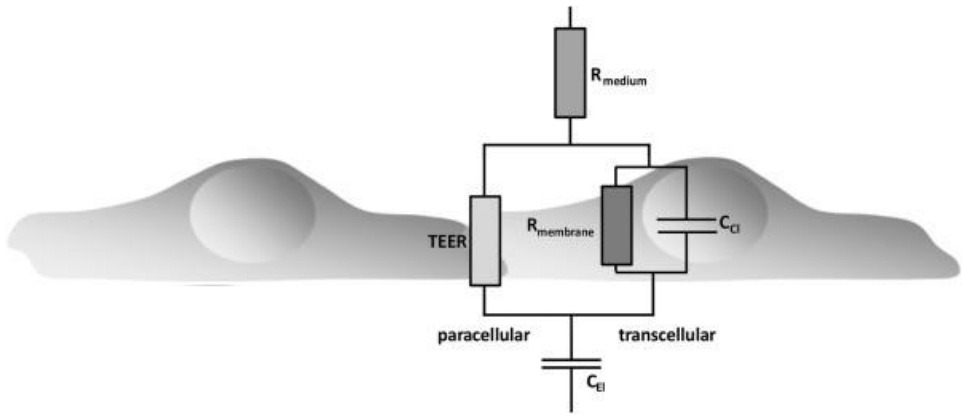


**Figure 7.** A representative circuit of an endothelial cell layer. The TEER representing the paracellular transport across the barrier is modeled as a resistor, while the transcellular transport is modeled as a parallel circuit of a resistor, $R_{membrane}$ representing the cell membrane, and a capacitor, $C_{Cl}$ representing the cell layer. The culture medium is modeled as a resistor, $R_{medium}$, and the electrode-medium interface as a capacitor, $C_{El}$. Reprinted from [57].

An example of an impedance spectrum can be seen in Figure 8. In Figure 8B a simplified circuit compared to the one shown in Figure 7 is seen. This simplification can be performed for the frequencies used for TEER measurements, as for this range the high resistance of the cell membrane will cause the current to mainly go through the capacitance representing the cell layer. For mid-range frequencies values the main contributors to the measured impedance are the TEER from paracellular pathways and the capacitance from the cells, and from this value the TEER can be extracted. Also in the case of an impedance spectroscopy a measurement from an empty membrane is needed and the resulting TEER value is normalized to the area [57]. Compared to a single frequency AC measurement the impedance spectroscopy is more accurate and sensitive in its measurements of the barrier integrity [58].

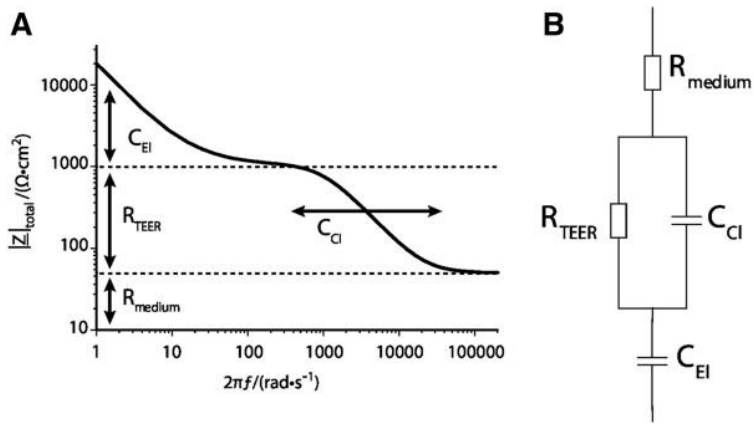


**Figure 8.** Schematic of an impedance spectra (**A**) together with a simplified electrical circuit of the endothelial cell monolayer (**B**). For different frequencies different components will affect the impedance the most. Low frequencies – capacitance of electrode and medium interface, middle-range frequencies – cell layer and for high frequencies – medium. Reprinted from [57].

### *2.2.4 Permeability assay*

As one of the defining characteristics of the BBB is the highly selective transport across the barrier, a common method to evaluate its integrity is by measuring the permeability of certain compounds across the barrier. In particular hydrophilic compounds have very restricted pathways across the barrier, and they either need to cross by specific transport proteins or through the paracellular pathways [59]. Therefore, hydrophilic compounds, typically labeled with fluorescent or isotope tracers, are often used for permeability assays. Commonly used molecules for permeability assays of the BBB are fluorescein isothiocyanate (FITC)-dextrans of different sizes [60]. These molecules are visualized with a fluorescent microscope in order to measure if they are capable of crossing the barrier, and the different sizes of the molecules are used to assess how tightly connected the cells are and to test the size-selectivity of the barrier, as the larger the molecule, the lower the chance is for it to cross the barrier [47].

# 3 Experimental background

In this chapter, some background information is included about the materials and methods used for the experiments described in the next chapters to help understanding the report. The chip design used is explained, followed by the characteristics of hydrogels and cell lines used for the experiments.

## 3.1 Chip design

The chip, previously developed at the BIOS Lab on a Chip group, consists of two connected PDMS parts, one top and one bottom, with a microchannel in each. At the crossing of the two channels a porous polycarbonate membrane is positioned, separating the channels. In connection to the channels from the edges of the chip are electrode channels where platinum electrodes are inserted, with a part of the electrode positioned in the fluid channel. The full design of the chip together with dimensions can be seen in Figure 9 [61].

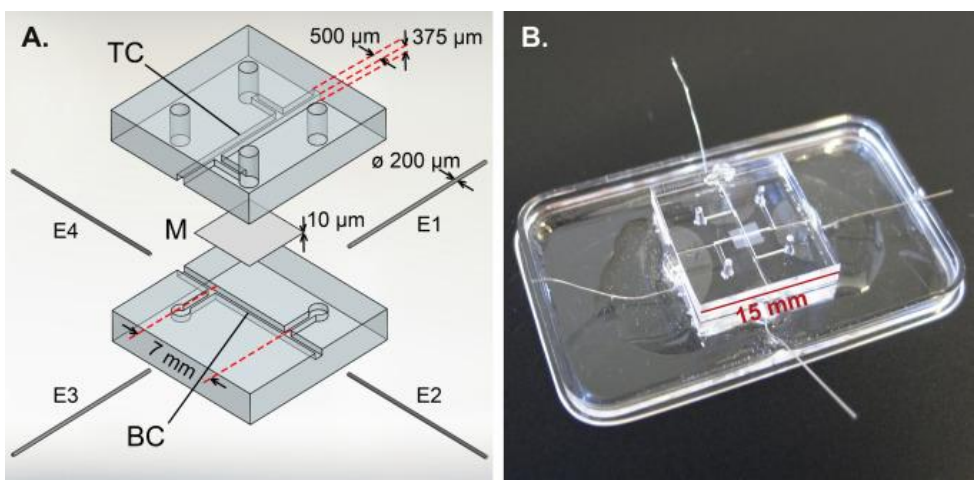


**Figure 9.** A schematic of the chip design (**A**) and an image of the assembled chip (**B**). In **A** the different parts and dimensions are presented. The chip consists of a top part containing a channel (**TC**) and holes for inlets and outlets of the channels. In the bottom part there is a channel perpendicular to the top channel (**BC**). Separating the two channels is a membrane (**M**) and four electrodes are incorporated, two in each channel (**E1-E4**). Reprinted from [61].

### *3.1.1 PDMS*

PDMS is an elastic polymer, commonly used for the production of biomedical microelectromechanical systems (BioMEMS), such as lab-on-a-chip and organs-on-chip. In most of the published BBB-on-chips, PDMS is the main component

used for chip fabrication [7, 53, 62]. The reason why PDMS is so extensively applied within this field is due to the fact that it is chemically inert, transparent, biocompatible, gas permeable, thermally stable, cheap and easy to handle [63].

Despite the large number of advantages using PDMS for these devices, the highly hydrophobic nature of the material can be a drawback, since interactions between the channel surface and the liquid used to create an aqueous environment for the cells will be low. This can be problematic during the filling of a chip with an aqueous liquid or when incorporating a hydrogel in the channel, causing detachment of the gel from the channel surface. Therefore, methods to increase the hydrophilicity and to incorporate reactive groups on the surface are desired [64]. The most commonly used method to achieve this is through plasma treatment. However, the hydrophilicity is short-lived, as the material resumes its hydrophobic state within a few minutes [65]. To create a more long-lasting effect different chemical surface treatments have been proposed in order to functionalize the PDMS, where some examples are polyvinyl alcohol (PVA), poly(ethylene glycol) (PEG) and (3-aminopropyl) triethoxysilane (APTES) treatments [67–69]. In the following sections the three different surface treatments used in the experiments are explained.

### *Plasma oxidation*

One method to increase the hydrophilicity of a PDMS surface is by oxidizing it, using plasma. This treatment will create hydroxyl groups on the surface, increasing the wettability of the surface. This is a short-lived surface functionalization, and the hydrophobicity will be restored [65].

### *Poly-L-lysine coating*

Poly-L-lysine (PLL) is a positively charged polyelectrolyte. When a PDMS surface is oxidized with plasma it will become negatively charged, causing the PLL to adsorb to the surface [69].

### *APTES and glutaraldehyde treatment*

For a more long-lasting treatment of PDMS a chemical treatment can be carried out. One method is through binding of APTES and glutaraldehyde (GA) to the PDMS surface, which will interact and covalently bond to proteins such as collagen. After oxidizing the PDMS surface the hydroxyl-groups will interact with the APTES, which will cross-link with the GA and in the final step create a

covalent bond to the protein [70]. A schematic of the treatment can be seen in Figure 10.

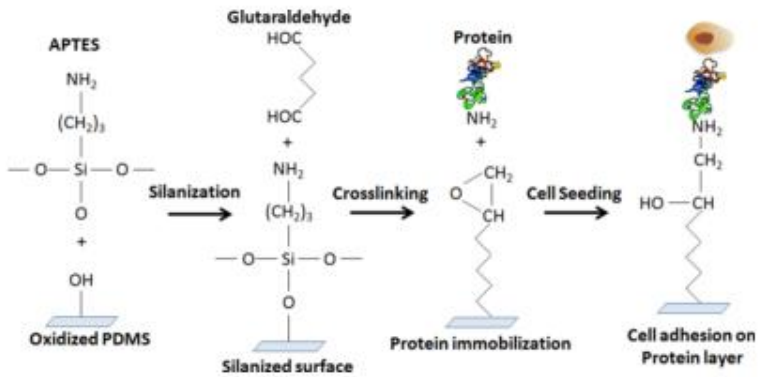


**Figure 10.** A schematic of the chemical treatment of a PDMS surface with APTES and GA, covalently binding to proteins. Reprinted from [70].

## 3.2 Hydrogels

Even though the standard procedure for cell culturing is on a 2D surface, experimental evidence shows that cells cultured on a 2D surface exhibit atypical behaviors when compared to the same cells *in vivo* [71]. Therefore there is an increased desire for *in vitro* culturing of cells in a 3D environment that resembles the natural environment of the cells. One promising type of material for creating these 3D environments is hydrogels, which are highly hydrated, cross-linked polymers [72]. These networks are capable of mimicking the ECM and can be made out of different materials. Typically the different polymers can be divided into two groups: synthetic polymers or natural polymers, depending on their origin. Some natural polymers used as hydrogels are collagen, HA and Matrigel and examples of synthetic polymers are 2-hydroxyethyl methacrylate (HEMA) and PEG [73].

In this project two different hydrogels were used. Further details about these are described below.

### *3.2.1 Collagen type I*

Collagen type I is one of the most abundant proteins in the ECM of humans and is commonly used as a natural polymer for hydrogels [74]. Collagen consists of

three amino acid chains that are arranged in a triple helical structure and assemble into fibrils and further into collagen fibers [75].

Collagen type I is one of the most commonly used hydrogels for culturing cells in BBB-models and it is mainly glial cells, such as astrocytes, and neuronal cells that are cultured within the gel [9]. Despite the fact that collagen type I is not a natural component of the ECM of the healthy brain, it is still widely used due to its strong cell adhesion and physical strength. In brain modeling it can be used to offer the support otherwise provided by neurons [76-77]. The collagen gels are typically stored in an acidic environment at 4°C, as they start to gel (meaning that the gel will go from liquid to semisolid) at a neutral pH or at room temperature [76].

Collagen is a natural protein and therefore typically extracted from animals. This will lead to a lower control of the reproducibility of the structure and mechanical properties of the gel, as well as batch to batch differences [78].

### *3.2.2 Hyaluronic acid*

HA, also referred to as hyaluronan, is a polysaccharide with a repeating unit of *N*-acetyl-D-glucosamine and glucoronic acid, and it can be found in the ECM throughout the whole human body, with the highest concentrations in soft connective tissue [79]. It is also one of the most abundant components of the ECM of the brain, together with proteoglycans and tenascins [39].

HA can be chemically modified to form hydrogels by addition of compounds to the functional groups of the chains, where some examples are thiols, aldehydes and haloacetate [80]. These hydrogels have a lot of different biomedical applications such as tissue engineering, drug delivery and cell culturing [76, 78, 80]. For cell culturing of brain specific cell types such as astrocytes, HA have been used to mimic the natural ECM of the brain [77].

## 3.3 Cells

Cells used for culturing can either be from immortalized cell lines, which are cell cultures from one original cell, primary cells, which are cells isolated from the body, or human induced pluripotent stem cells, adult cells that has been converted into pluripotent stem cells. The cells can be obtained from different sources such as pig, rat, cow and human. For BBB research a lot of different cell lines are available and they exhibit different properties, making some cell lines more suitable for certain studies than others. The cell lines used for the study explained in this report are explained in further detail in the following sections.

### *3.3.1 hCMEC/D3*

The human cerebral microvascular endothelial cells hCMEC/D3 are a cell line of primary endothelial cells, obtained from the brain, which has been immortalized (kindly provided by Dr. P.-O. Couraud, INSERM, Paris, France) [82]. This allows the cells to maintain the BBB specific properties of cerebral endothelial cells as well as increased survival in an *in vitro* environment. The hCMEC/D3 cell lines typically express cerebral endothelial cell morphology and tight junction markers such as ZO. However, the TEER values are on average 40 $\Omega cm^2$ in standard cultures, which is significantly lower than *in vivo* values of more than 1000 $\Omega cm^2$. When co-cultured with other cell types the TEER value is either slightly increased, with astrocytes, or not affected at all, with pericytes [49].

### *3.3.2 Primary human astrocytes*

Primary human astrocytes are isolated from the human brain. For the cells used in the experiment presented in this report they are specifically from the cerebral cortex (ScienCell, Catalog 1800). The cells are isolated from a brain sample and purified for astrocytes by removing the other cell types present in the brain sample [83]. For primary cell cultures the same function and expression of the cell type *in vivo* is obtained. However, the main limitation of these cells are their low doubling capacity, meaning that they can only be used for lower passage numbers (for the cells used in this experiment a passage number below 10 was always used) [84].

## 3.4 Measurement methods

In order to characterize the outcome of each experiment two different methods were used. In all experiments the cells were stained in order to evaluate morphology, viability and expression and in the final experiment a TEER measurement was performed to evaluate the barrier integrity of the endothelial cells.

### *3.4.1 Staining*

Visualization of cells through the addition of fluorescent compounds is one of the most important methods to evaluate structure and function of cells [85]. There is a wide range of different stainings that will stain different structures of the cell, where some examples are the nucleus, cytoskeleton and membrane. For the experiments presented in this report staining of nucleus, actin filaments and GFAP were performed.

For staining of the nucleus NucBlue was used. NucBlue contains the label Hoechst 33342, a compound with high membrane permeability that emits fluorescent light at a wavelength of 460 nm (blue) when bound to DNA (Invitrogen). Staining of the nucleus was performed for detection and counting of cells.

To visualize the morphology of cells actin filaments, which makes out part of the cytoskeleton of cells, are targeted. Two different actin stainings were used for the experiments, ActinGreen and Texas red-X Phalloidin. Both stainings contain a probe with high affinity for actin filaments that has been combined with a fluorescent dye. ActinGreen contains the green fluorescent dye Alexa Fluor 488 and Texas red-X Phalloidin contains the red fluorescent dye Texas red (Invitrogen).

Staining of GFAP requires indirect staining with antibodies. For indirect antibody staining a primary antibody, commonly produced in an animal such as rat or mouse, is added that binds specifically to the desired antigen, in this case GFAP. Afterwards, a secondary antibody labeled with a fluorescent dye, directed against the primary antibody, will be applied to the sample. Important for the secondary antibody is that it has to be produced in another animal, against the first animal [86]. For the experiments presented in this report rat anti-GFAP was used as primary antibody and either goat anti-rat IgG Alexa Fluor 568 or 488 as secondary antibody.

### *3.4.2 TEER setup*

The TEER was measured using a model designed and fabricated in-house (commercialized as Boxense by LocSence, Enschede, the Netherlands) and the setup can be seen in Figure 11. A laptop containing a Labview program written in-house operates a lock-in amplifier. The amplifier is connected by two clamps to the electrodes of the chips (Figure 12). A total of six measurements for six different connection combinations to the platinum electrodes are performed for each chip. The impedance spectroscopy was screened over frequencies between 200 Hz-1 MHz in 100 steps.

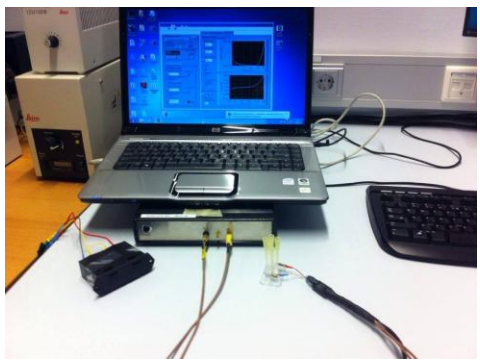

**Figure 11.** Image of setup used for TEER measurements. In the image a black lock-in amplifier box containing a signal generator and measurement equipment, a computer with the Labview program and a probe with an additional amplifier circuit connected to the chip with two clamps are shown.

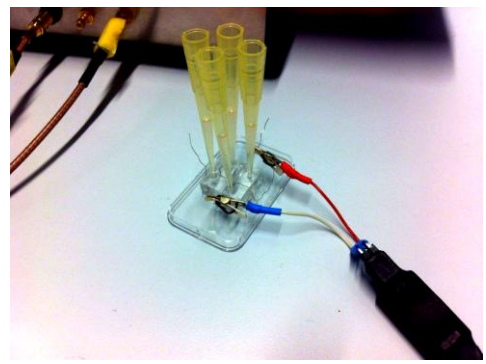

**Figure 12.** Zoom in of the chip and its connection with the probe. In the image the clamps are attached to two of the electrodes.

From the measurements the bode plots together with raw data containing output voltage, phase shift and input voltage for each connection can be extracted and is loaded into a Matlab script [87]. The channels filled with medium and the membrane with cells can be represented by resistors, shown schematically in Figure 13. From the raw data the impedance of each connection is calculated resulting in the formation of six linear equations, one for each connection. By solving these equations the membrane resistance is obtained (see equations 4-10) [87].

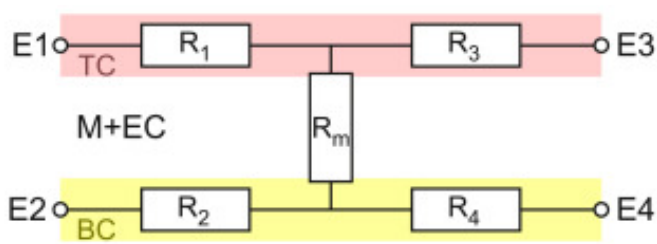


**Figure 13.** Simplified electrical circuit of the chip. The top channel (**TC**), connected to electrode 1 and 3 (**E1** and **E3**), is represented by the resistors $\mathbf{R_1}$ and $\mathbf{R_3}$ and bottom channel (**BC**), connected to electrode 2 and 4 (**E2** and **E4**), is represented by the resistors $\mathbf{R_2}$ and $\mathbf{R_4}$. The membrane (**M**) together with the endothelial cell layer (**EC**) is represented by one resistor ($\mathbf{R_m}$). Reprinted from [61].

$$R_{13} = R_1 + 0 + R_3 + 0 + 0 \quad (4)$$

$$R_{24} = 0 + R_2 + 0 + R_4 + 0 \quad (5)$$

$$R_{12} = R_1 + R_2 + 0 + 0 + R_m \quad (6)$$

$$R_{14} = R_1 + 0 + 0 + R_4 + R_m \quad (7)$$

$$R_{34} = 0 + 0 + R_3 + R_4 + R_m \quad (8)$$

$$R_{23} = 0 + R_2 + R_3 + 0 + R_m \quad (9)$$

These six equations can be summarized into the following equation for $R_m$:

$$R_m = 0.25 * (R_{12} + R_{14} + R_{34} + R_{23} - 2R_{13} - 2R_{24}) \quad (10)$$

where $R_m$ is the total resistance of the cell layer and the membrane [87]. For the hCMEC/D3 cell line there will be a high paracellular transport, making the transcellular transport negligible. Therefore, to obtain the TEER from the total resistance only the resistance of the membrane, measured on the blank chip, needs to be subtracted. Finally, the resulting resistance value is normalized to the surface area, as explained in section 2.2.3.

# 4 Experiment 1: Surface functionalization

The hydrophobic nature of PDMS makes it a problematic material to use when working with hydrogels, due their high water content. With low interaction between gel and channel wall, the risk of gel contraction and failure of the structure increases when external forces such as fluid flow and internal forces from cells are added. To increase the interaction between the hydrogels and PDMS channels, three different surface treatments of the channels have been evaluated.

## 4.1 Materials and methods

For the experiment a total of 8 chips were used to evaluate three different surface treatments. A simplified design of the PDMS chip explained in section 3.1 with a single channel connected to a PDMS-coated glass cover slip, seen in Figure 14, was used (for method see appendix A. Chip fabrication). The three different surface treatments evaluated are: plasma oxidation, PLL coating and a chemical treatment with APTES and GA. Untreated chips were used as control. The protocols for the different treatments are described in the sections below.

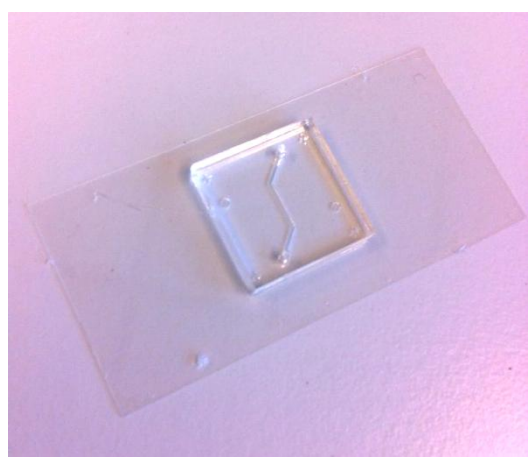

**Figure 14.** Image of the chip design where a single-channel PDMS chip has been plasma bonded to a glass cover slip coated with a thin layer of PDMS.

To functionalize the surface of the PDMS channel with plasma oxidation three chips were plasma oxidized at a low radio frequency (RF) setting for 40 s (Plasma cleaner/sterilizer, Harricks). After the plasma treatment two of the chips were stored at 4°C for 3 h before adding the hydrogel, and the third chip was filled with the gel directly after it had been treated with plasma.

To add a coating of PLL to the surface of the channel one chip was plasma treated at a low RF setting for 40 s and directly after filled with a PLL solution of 1 mg/ml (ScienCell Research Laboratories). The chip was incubated at room temperature for 2 h and afterwards the solution was aspirated. Prior to adding the hydrogel, the channels were rinsed with sterile purified water. Inspired by protocol from [88].

For the chemical treatment of the PDMS surface a 3% APTES (Sigma Aldrich) solution in MilliQ (Purelab Flex) was pipetted into the channels of two chips, which were left to incubate at room temperature in the solution for 30 min. Afterwards they were rinsed in 99% ethanol (Boom) and left to incubate in ethanol at room temperature for another 30 min. Once more the chips were rinsed with ethanol and then dried with an air blow gun. In the final step a 20% GA (Sigma Aldrich) solution in phosphate-buffered saline (PBS) was pipetted into the channels and left in the solution to incubate at room temperature for 30 min. After the final incubation step the chips were rinsed with purified water and dried with an air blow gun. The chips were stored at 60°C over-night. Based on protocol from [70].

For the hydrogel a collagen type I concentration of 3 mg/ml and an astrocyte concentration of $5.5 \cdot 10^6$ cells/ml at a passage number of 7 were used in all chips (for method on cell culturing see appendix A. Cell culturing).

To neutralize and dilute the collagen type I stock 10X PBS and 1 M NaOH (Sigma Aldrich) were added to an Eppendorf tube and put on ice. Astrocyte medium (AM: Lonza) containing the cells to be seeded in the gel was added to the tube and in the final step the collagen type I (Corning) was added (concentrations and volumes used are found in appendix A. Hydrogels). The liquid gel was mixed thoroughly through pipetting and then added to the channels. The chips were left in an incubator at 37°C for 30 min to be sure of complete gelling before adding fresh AM. The medium was changed by inserting a pipette tip in the inlet containing 150 µl and another pipette tip in the outlet containing 100 µl. The hydrostatic pressure difference between the pipette tips ensures a slow flow rate of fresh culture medium through the channel. Medium was changed twice per day, once in the morning and once in the afternoon, during the 48 h duration of the experiment. Images were taken at 24 h and 48 h with a phase contrast microscope (EVOS FL Cell Imaging System).

As a final step the cells were fixated and stained with ActinGreen and NucBlue and imaged using a fluorescent and confocal microscope (Nikon Confocal A1). For protocol of staining see appendix A. Staining of cells and for more information about microscopy see appendix A. Microscopy.

## 4.2 Results and discussion

Out of the eight chips that were filled with cell-seeded hydrogels, one of the glass cover slips broke when adding the hydrogel and was not used further. After 24 h, in three of the chips the gel was for the most part attached to the walls and in the other four chips the gel had detached from the walls. After 48 h of the experiment only in one of the chips the gel was still attached to the channel walls and in the other two the gel had detached. A summary of these results can be seen in Table 1 and images showing examples of gels attached and detached from the walls can be seen in Figure 15 and 16.

**Table 1.** Table summarizing the outcome of each chip with different surface treatments at the two different time frames of the experiment, 24 h and 48 h. A-gel attached, D-gel detached, X-damage to chip and S-staining.

| | No surface treatment | | APTES + GA | | Plasma oxidation, stored 4°C | | Plasma oxidation | PLL coating |
|---|---|---|---|---|---|---|---|---|
| Chip number | 1 | 2 | 3 | 4 | 5 | 6 | 7 | 8 |
| 24 h | A | D | A | X | A | D | D | D |
| 48 h | D | - | S | - | D | - | - | - |

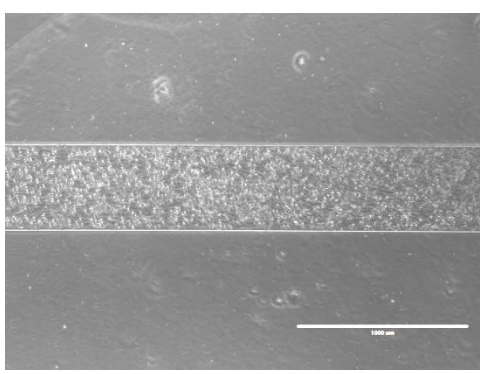

**Figure 15**. Image of chip 3 at 24 h showing a gel attached to the channel walls. Taken with phase contrast microscope with a scale bar of 1000 µm.

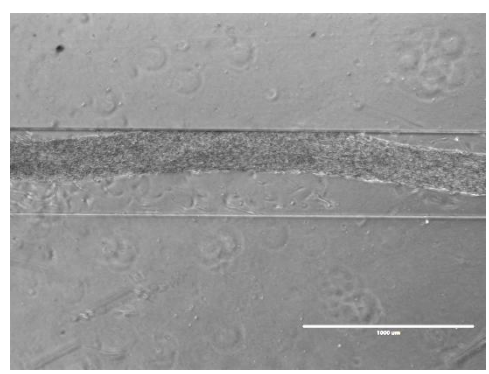

**Figure 16.** Image of chip 2 at 24 h showing a gel detached from the channel walls. Taken with phase contrast microscope with a scale bar of 1000 µm.

For the chip chemically treated with APTES and GA the gel was still fully attached to the walls after 48 h. This chip was used for staining and viable cells with characteristic morphology of astrocytes could be seen (Figure 17 and 18).

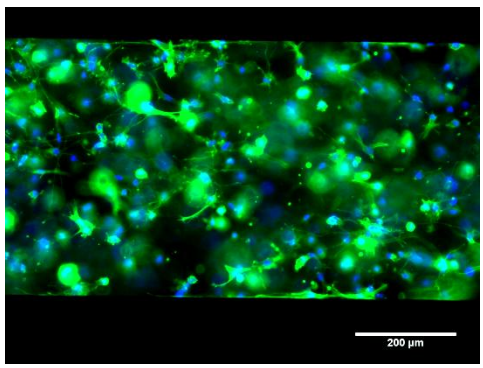


**Figure 17.** Image from chip 3, treated with APTES and GA, showing astrocytes distributed in the gel inside the channel. The cells were stained with NucBlue and ActinGreen and imaged with GFP and DAPI filter cubes. Scale bar is 200 µm.

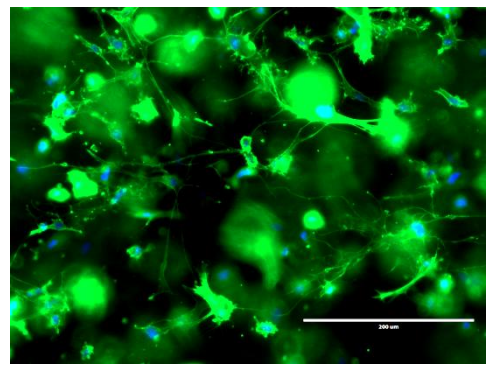

**Figure 18.** Image from chip 3 with higher magnification showing star-shaped astrocytes. The cells were stained with NucBlue and ActinGreen and imaged with GFP and DAPI filter cubes. Scale bar is 200 µm.

With confocal microscopy it was possible to see that the gel was attached to the channel walls in its full height and that the cells were spread throughout the gel, as seen in Figure 19 and 20. In Figure 20 the height of the gel is seen, where the intensity of the cells is higher on the left side (bottom of gel) compared to the right side (top of gel). This is due to the confocal microscope where the excitation laser is placed underneath the sample, causing a lower intensity from the cells positioned higher up in the sample, meaning further away from the laser. However, cells can still be distinguished on the right side, proving the distribution of cells throughout the gel.

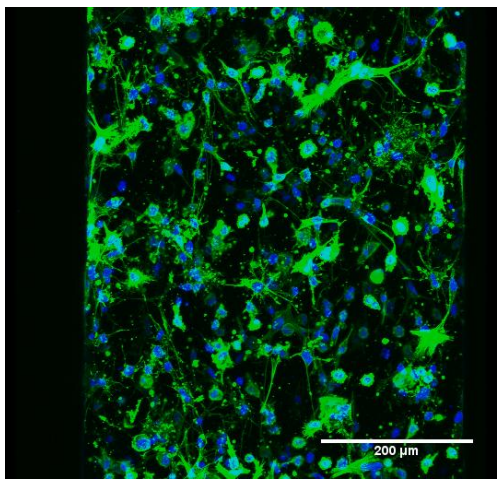


**Figure 19.** Image of the channel in chip 3, treated with APTES and GA, from the top. Taken with confocal microscopy. Scale bar is 200 µm.

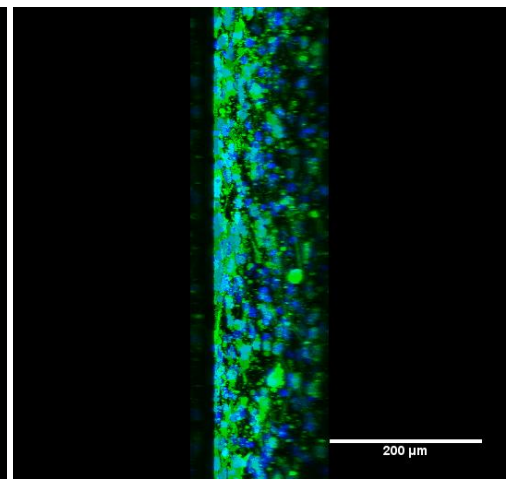


**Figure 20.** Image of the channel in chip 3 from the side. Taken with confocal microscopy. Scale bar is 200 µm.

During the experiment most of the gels detached from the channel walls and the only chip in which the gel was still attached was the chip treated with APTES and GA. The reason for the high interaction between walls and gel when treated with APTES and GA is that the GA gets covalently bonded to the proteins in the hydrogel, creating a strong connection [89]. However, it is worth noting that the protocol for the APTES and GA treatment is more extensive than the other two protocols used in this experiment. Several sources have used PLL coatings and plasma oxidation for successful gel attachment to PDMS [5, 87, 90]. The degree of gel contraction typically depends on three different factors: collagen concentration, mechanical strength of the gel and cell density [91]. By varying one of these three parameters gel contraction can be decreased or completely avoided. An example of this is found in the article by Adriani et.al [9]. When using a pre-coating of poly-D-lysine and a low collagen concentration, gel contraction occurred. After increasing the collagen concentration of the gel, they did not have further problems with gel contraction [9]. Intentionally for this experiment, conditions were chosen so that high forces, due to a high cell concentration, would be exerted on a relatively weak matrix. This decision was made to ensure that the treatment chosen was sufficient to avoid gel contraction in later experiments, where the hydrogel concentration was to be varied.

Due to the number of chips tested for each condition (between one and three chips), the reliability of the results are low. However, for this study it was chosen to rely on the results obtained from this experiment for further use.

## 4.3 Conclusion

The aim of this experiment was to incorporate a hydrogel seeded with astrocytes in a microfluidic channel. To ensure high interaction between the PDMS-chip and the hydrogel, different surface treatments were evaluated. From the results obtained, the APTES and GA surface treatment proved strong connection. Due to these results the APTES and GA surface treatment was used for incorporation of hydrogels in microfluidic chips in later experiments.

# 5 Experiment 2: Hydrogel composition

Astrocyte structure and function are dependent on the environment that they are cultured in. When cultured in 2D they adopt a stretched out morphology, atypical for *in vivo* astrocytes, and a high GFAP expression, which is a feature of reactive astrocytes. However, when cultured in 3D they show characteristic star-shaped morphology and a low GFAP expression, typical for their non-reactive state. Furthermore, it is assumed that the composition of the 3D culture environment may have an effect on cultured astrocytes. It has been reported that astrocytes tend to be less reactive when cultured in a collagen type I and HA hydrogel compared to when cultured in only collagen type I, and that also the ratio between collagen and HA concentrations will influence the reactivity. Therefore, an investigation on astrocyte morphology and reactivity when cultured at different collagen type I and HA concentrations was performed. The investigation will be carried out through image analysis where the intensity of GFAP expression was measured, shape of the cells was evaluated and number of processes was counted.

Astrocytes seeded in different hydrogel composition were added to 12 microfluidic chips. After 48 h the cells were stained in order to evaluate morphology and reactivity. Unfortunately, the viability of the cells was low. Since the amount of data obtained from the experiment was insufficient to draw any conclusions, it was decided to repeat the experiment with some changes to the method. It was hypothesized that the reason for the low viability was a combination of low cell concentration and high medium flow. Since astrocytes had already been cultured successfully in hydrogels in chips in previous experiments, the method was simplified in order to shorten time, by instead using a 96 wells plate for 24 h. Details about the method and results from the experiment carried out in chips can be found in appendix B. Hydrogel composition in chips, while in this section the experiment performed in a 96 wells plate are presented.

## 5.1 Materials and methods

In total, 18 wells to test nine conditions (2 wells/condition) were used for this experiment. In four of the conditions the collagen type I and HA concentrations were varied based on ratios found in literature [77, 92]. For positive controls culture conditions where astrocytes were more reactive were desired. Two conditions were used as positive controls for GFAP expression, astrocytes cultured in a collagen type I gel and on a 2D surface, and three conditions were

added as control for the antibody staining. In all hydrogels an astrocyte concentration of $1.0 \cdot 10^6$ cells/ml was used at a passage number of 8 and astrocytes and endothelial cells cultured in 2D were seeded at a concentration of $3.0 \cdot 10^4$ cells/$cm^2$. In the wells where endothelial cells (passage number 34) were to be cultured the surface was pre-coated with 40 µg/ml fibronectin for 1 h. In Table 2 the different conditions and stainings used in the experiment can be found. As the stainings for actin and nucleus was applied to all conditions, they are not included in the table.

**Table 2.** All conditions are summarized in the table. In the table the following information is provided; cell type (A – astrocyte and E – endothelial cells), collagen type I concentration, HA concentration, addition of primary antibody and secondary antibody.

| Condition | 3D C 4 | 3D C:HA 3:1 | 3D C:HA 4:1 | 3D C:HA 5:1 | 3D C:HA 4:2 | 3D C:HA 3:1 | 2D Astro | 2D Ab | 2D EC Ab |
|---|---|---|---|---|---|---|---|---|---|
| Cell type | A | A | A | A | A | A | A | A | E |
| Collagen mg/ml | 4 | 3 | 4 | 5 | 4 | 3 | - | - | - |
| HA mg/ml | - | 1 | 1 | 1 | 2 | 1 | - | - | - |
| Primary Antibody | + | + | + | + | + | - | + | - | + |
| Secondary Antibody | + | + | + | + | + | + | + | + | + |

All the gels were made according to the following protocol though with varying volumes depending on the condition (see appendix A. Hydrogels). 10X PBS, 1M NaOH and AM were added to Eppendorf tubes and put on ice. As preparation, HA was mixed with poly(ethylene glycol) diacrylate (PEGDA; Glycosan HyStem Trial Kit) at a ratio of 1:4 according to manufacturer's recommendations. The appropriate volumes of collagen type I and HA were added to the tubes. In the final step the cells were detached from the culture flasks and resuspended in AM and added to the Eppendorf tubes. After mixing of the liquid gel through pipetting, 50 µl was added to each well. Endothelial cells and astrocytes cultured in 2D were added to the wells together with endothelial cell growth medium (EGM-2) or AM. The gels were left to incubate at 37°C for 30 min, to ensure proper gelation, before 50 µl AM was added to the wells.

Medium was refreshed twice during the 24 h experiment by removing old medium through pipetting, and new medium was added in the same way. Time frames were taken at 4 h and 24 h with phase contrast microscopy. After 24 h the cells were fixated and stained with Texas red-X Phalloidin, NucBlue, primary

antibody rat anti-GFAP and secondary antibody goat anti-rat IgG Alexa Fluor 488 (see appendix A. Staining of cells) and imaged with fluorescent microscopy.

### *5.1.1 Image analysis*

To obtain a representative and concise set of images, a plane approximately in the middle of the height of the gel was chosen and fixed for all samples. All images were taken at 10 times magnification and the intensity levels for the three filter cubes used were fixed at 30% for the green fluorescent protein (GFP) filter cube, at 40% for the 4',6-diamidino-2-phenylindole (DAPI) filter cube and at 40% for the red fluorescent protein (RFP) filter cube. There were two wells for each condition and from each well four frames were taken, making a total of eight frames for each condition. The position of each frame was chosen with the DAPI filter cube where the staining of the nucleus was shown and neither morphology nor GFAP-expression was distinguishable to prevent biased interpretation. In each position an image from each of the three filter cubes mentioned before was obtained. An example of such a set of images is seen in Figure 21A-C.

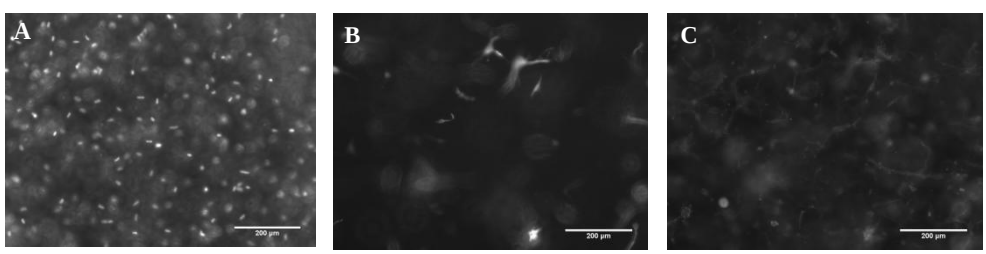


**Figure 21.** In **A-C** an example of a frame taken with the three different filter cubes is shown; DAPI, GFP and RFP. In **A** the staining of nuclei is shown, in **B** the GFAP staining is visible and in **C** the actin staining. Scale bar is 200 µm.

For image analysis the program ImageJ (1.48v, National Institutes of Health) was used. In the first step the number of cells present in the image was counted by hand. To do this, the image taken with the DAPI filter cube, showing the nuclei, was used. Firstly, the background noise was subtracted from the image using a rolling ball algorithm with the largest size radius set at 12 pixels. This value was optimized for the removing of background noise while maintaining information about cells close to the focal plane through testing of different radii sizes. Afterwards, a threshold for the intensity was set at 98% intensity for all images. Examples of a frame after the different steps had been carried out, together with the original frame, can be seen in Figure 22. From Figure 22C the number of cells was counted and only the cells visible in this frame were included during the rest

of the analysis. If the nucleus of a cell was not seen in this image, it was not used for the analysis.

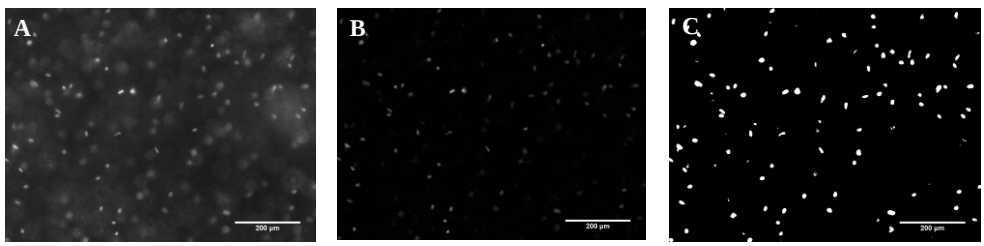


**Figure 22.** In **A-C** three images are shown after subsequent steps performed during the image analysis. In **A** the original image taken with the DAPI filter cube shows the nuclei with a high background noise. In **B** the same image as **A** is shown after the background intensity has been subtracted. In **C** a threshold of the intensity has been set for the image shown in **B**. Scale bar is 200 µm.

In order to distinguish cells expressing GFAP and with a visible nucleus, an overlay of the two images was created. Afterwards, from the frames taken with the GFP filter cube, cells were divided into "in focus cells" and "out of focus cells". This division was decided by the clarity of the cell body, where an example of a cell in focus can be seen in Figure 23A and a cell out of focus in Figure 23B. To analyze the GFAP expression for these cells it was needed to measure the fluorescence intensity and minimum intensity in the frame, which represented the background noise. In ImageJ the measurements were set to give the average intensity and minimum intensity per pixel. The cell shape was then drawn out with the use of the freehand drawing tool and the measurements were performed on this figure. Examples of the freehand drawing for a cell in focus and a cell out of focus can be seen in Figure 23C and D. For background noise the minimum intensity of the whole image was measured.

For analysis of the morphology of the cells the frame taken of the GFAP staining was used and the visible cells were divided into two groups based on their morphology; star-shaped or elongated. The number of primary processes for cells defined as star-shaped was counted. Primary processes are processes that originate from the cell body, and in Figure 23A a primary process has been marked.

To evaluate if the results of the average GFAP expression between conditions were statistically significant a Student's *t*-test was performed. Comparisons were performed between all conditions for the total cells category. *P* values below 0.05 were considered statistically significant.

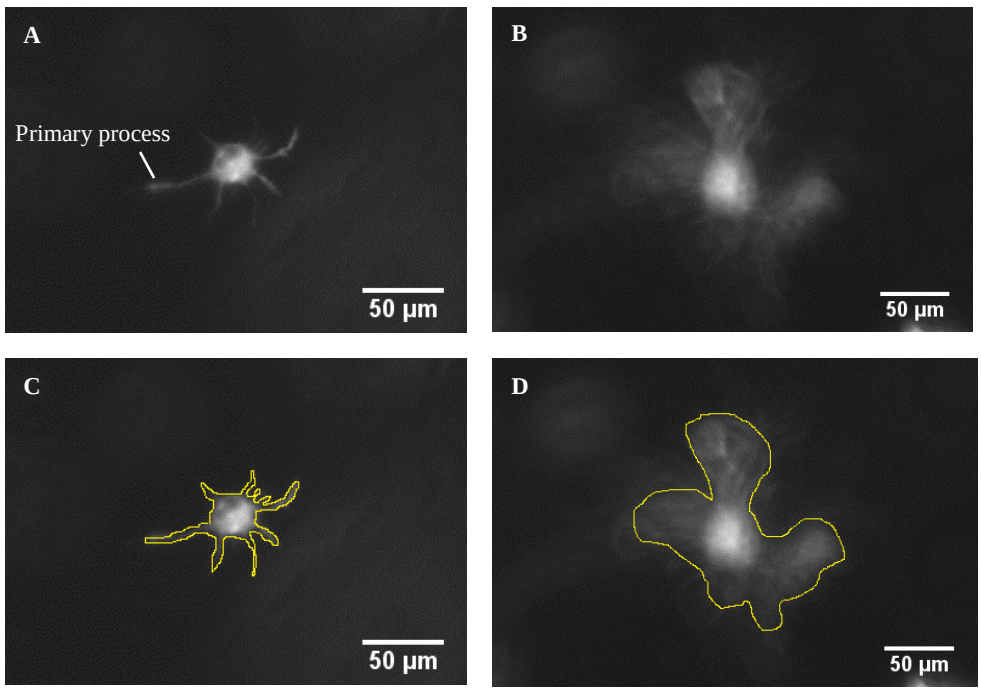


**Figure 23.** In **A** a cell defined as in focus is shown and a primary process is marked out while in **B** an example of an out of focus cell is shown. In **C** and **D** examples of freehand drawing on cells in and out of focus are shown. All images are taken with the GFP filter cube showing GFAP expression, and displayed in grey scale. Scale bar is 50 µm.

## 5.2 Results and discussion

The hydrogels and cells were added to the wells and cultured successfully for 24 h. Although in two wells a bubble was incorporated in the gel, the effect on the gel was very low and no extra measures were taken. After 24 h the cells were fixated and stained. While the cells in the gels remained in place, during the staining some of the cells grown in 2D were washed away. Images from all wells were taken for analysis and examples of frames from each condition can be seen in Figure 24.

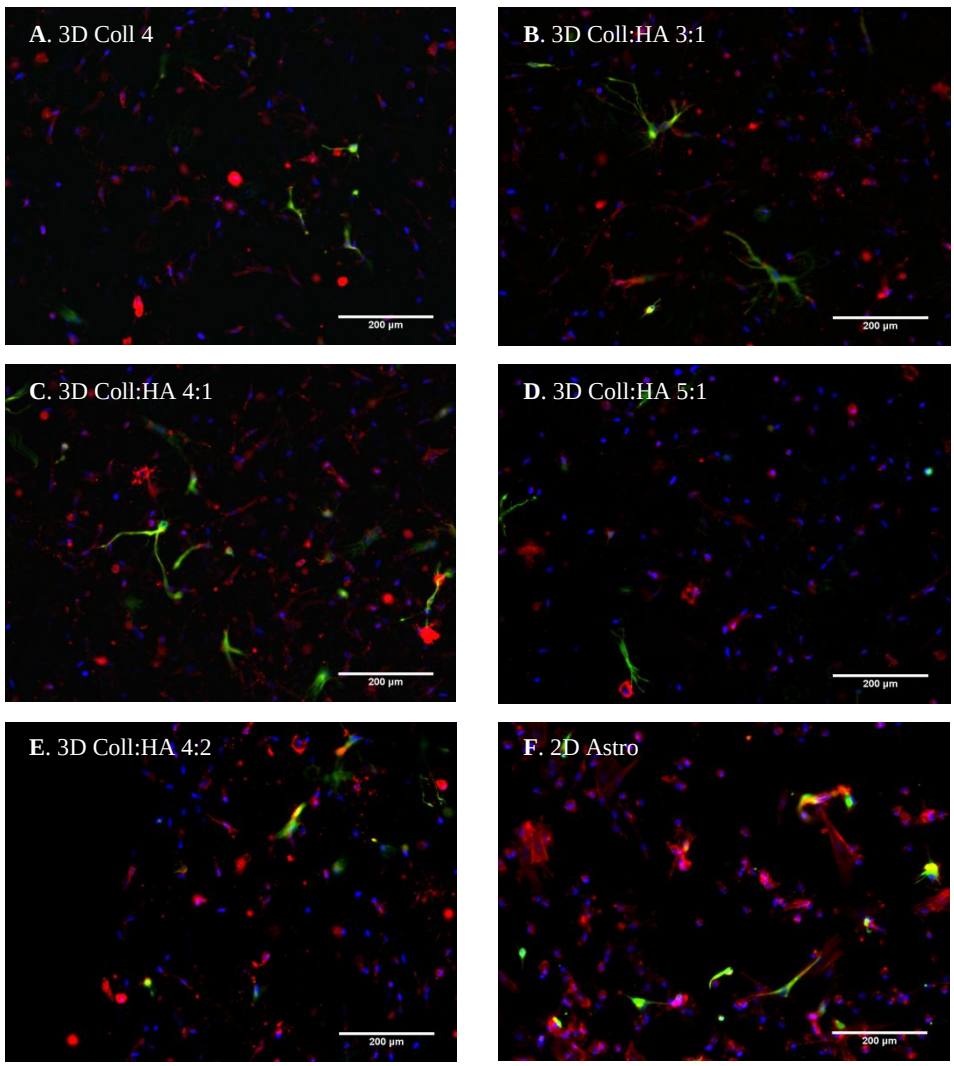


**Figure 24.** In **A-F** representative images from each condition used for analysis is shown as overlays of the three images taken with the three filter cubes; RFP, DAPI and GFP. Red is actin, blue is nucleus and green is GFAP. Consist for all images is that there is a high nuclei density where actin filaments are distinguishable, although the majority of these cells exhibit an elongated morphology. GFAP expression is distinguished for a low number of cells, however a larger amount of these cells have a star-shaped morphology Scale bar is 200 µm.

What is seen in most frames is that there is a large number of cell nuclei visible together with a weak signal for actin. The signal for GFAP is strong in some cells, however from most cells there is no detectable signal. This large variation in signal levels for the actin and GFAP staining is especially visible by comparing the stainings in the same well with a lower magnification, which can be seen in Figure 25 and 26. From the GFAP staining a large number of star-shaped astrocytes are distinguishable from the background, while in the image showing the actin staining it is hard to distinguish cell structures from the background and from each other. This could be seen in all the wells, and due to the high background noise and difficulties to distinguish structures from the actin staining it was chosen not to use images taken with the RFP filter for the analysis.

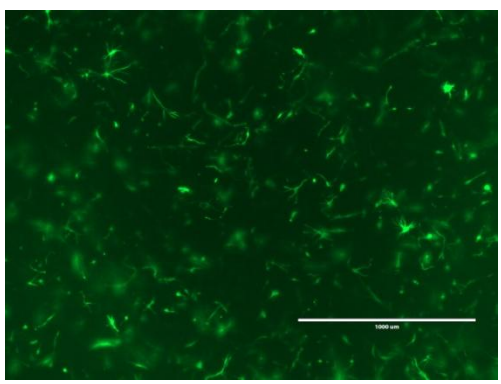

**Figure 25.** Image showing the GFAP staining in a gel. Imaged with GFP filter cube and the scale bar is 1000 µm.

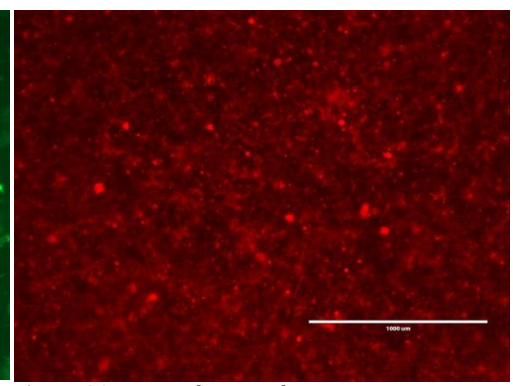

**Figure 26.** Image showing the actin staining in a gel. Imaged with RFP filter cube and the scale bar is 1000 µm.

The analysis was performed to gain information about the reactivity of astrocytes in different gel compositions. Therefore, data about the average GFAP intensity per cell, number of GFAP positive astrocytes and the total amount of cells was obtained. In Graph 1 the percentage of total amount of cells expressing detectable levels of GFAP is shown. These results indicate a very low degree of GFAP-positive astrocytes with a highest value of 6.9 % and lowest of 3.6 % of the total number of cells.

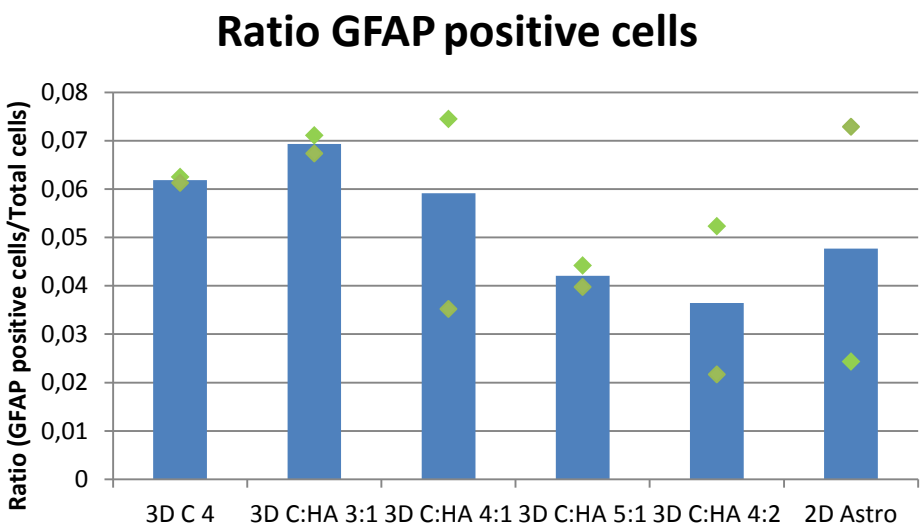


**Graph 1.** In the graph the ratio of GFAP positive cells against the total amount of cells is shown for the five gel conditions and the 2D condition. The blue bars show the total ratio of all the cells for a condition, while the green diamonds show the ratios for each of the two wells per condition. The highest percentage of GFAP positive cells was found in the 3 mg/ml collagen type I and 1 mg/ml HA gel and the lowest in the gel containing 4 mg/ml collagen type I 2 mg/ml HA. The ratios differ between 0.069 and 0.036.

In Graph 2 the average GFAP expression per cell for each condition can be seen, where cells have been sorted in three categories: “in focus”, “out of focus” and “total cells”. From this graph it can be distinguished that the lowest average GFAP expression is in the only collagen type I gel. From the Student’s *t*-test the average GFAP expression of cells grown in 3D C 4 and 3D C:HA 3:1 were significantly lower than the other conditions (except between 3D C:HA 3:1 and 3D C:HA 4:2 where no statistical difference was found), however between the two conditions there was no statistically significant difference.

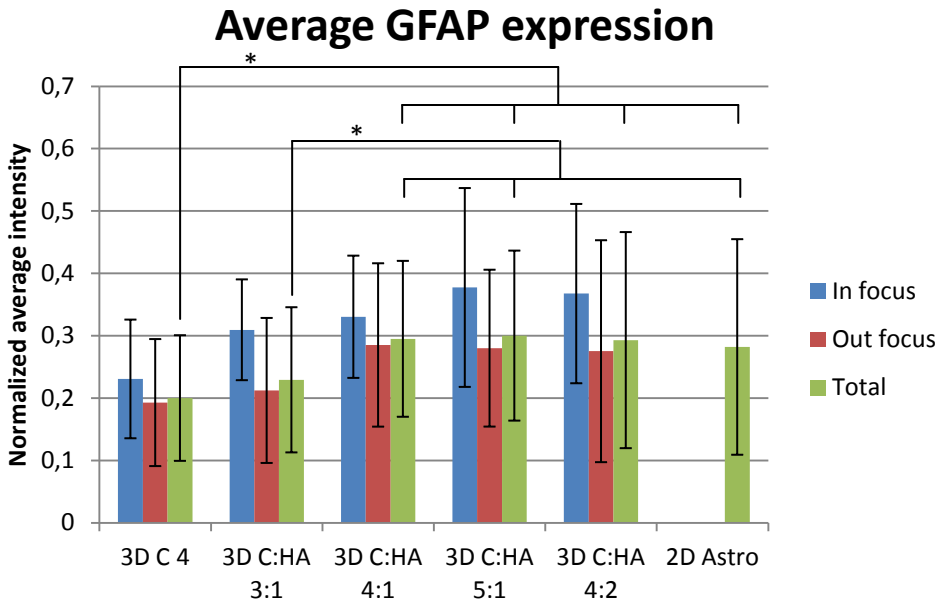


**Graph 2.** In the graph the average intensity per cell is shown for the five different gel conditions and the 2D condition. The bars are divided into "in focus cells", "out of focus cells" and "total cells". Since all the cells were in focus in the 2D condition only a "total cells" bar is shown. Average intensity is obtained from the average pixel intensity for each cell normalized to the maximum pixel intensity. Both for average and maximum intensity the background intensity was subtracted. The standard deviation was determined from the average intensity with background noise subtracted, over all the cells for one condition. From the graph it is seen that the lowest GFAP expression for all three groups is found in cells grown in the 4 mg/ml collagen type I gel. Statistical significance was determined with a student's *t*-test between the averages of total cells for all conditions. *$P \leq 0.05$.

The second parameter to be investigated is the morphology of the cells with respect to shape and number of primary processes. In Graph 3 the obtained results about the morphology of the cells has been summarized. In the graph it can be seen that a high percentage of the cells analyzed exhibits the star-shaped morphology, characteristic for astrocytes. However, more than half of the cells in all gels have fewer than 10 primary processes, which is a low number in comparison to other cultured astrocytes [77].

For the analysis of morphology the original idea was to analyze images showing the actin staining. Due to the high background noise it was decided to instead use the images taken of the GFAP staining, which decreases the amount of data as very few cells expressed detectable levels of GFAP (see Graph 1). Furthermore, to be able to analyze the morphology the cells needed to be close to the focal plane in order to distinguish its shape and the processes, decreasing the number of

suitable cells further. For these reasons the number of cells analyzed is too low to be statistically relevant.

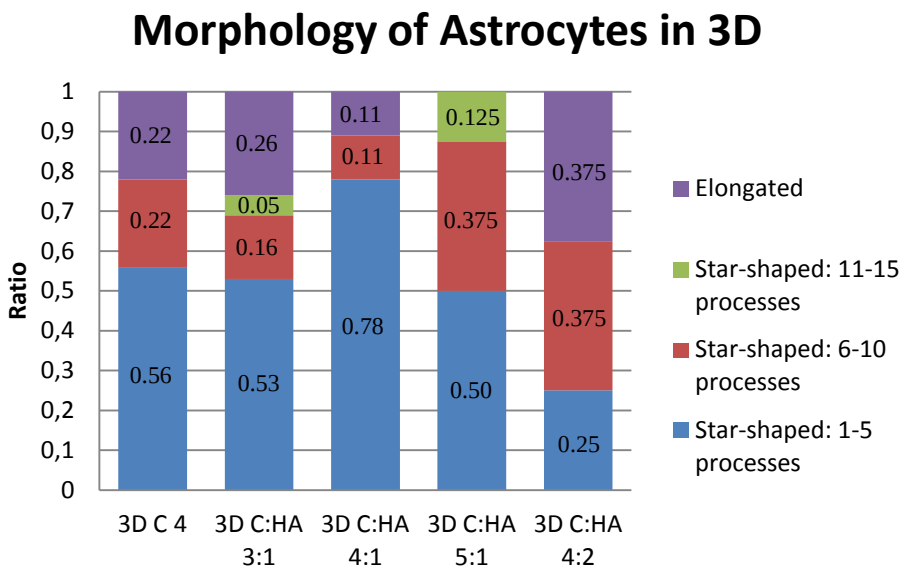


**Graph 3.** In this graph the morphology of GFAP positive cells have been summarized into four categories: cells with a star-shaped morphology and 1-5 processes (blue), cells with star-shaped morphology and 6-10 processes (red), cells with star-shaped morphology and 11-15 processes (green) and cells with an elongated shape (purple). For each condition the ratios of cells in each category has been divided with the total amount of cells used in the analysis for that condition. The total number of cells (N) for each condition are: $N_{C4}$=9 cells, $N_{C:HA3:1}$=19 cells, $N_{C:HA4:1}$=9, $N_{C:HA5:1}$=8 and $N_{C:HA4:2}$=8.

The results obtained from the analysis of GFAP expression indicate that the addition of HA to the hydrogel composition of cultured astrocytes does not necessarily decrease the reactivity of astrocytes. These results contradict the results found in another study, where a significant difference was presented [77]. Before a conclusion is drawn, the limitations of the used method and possible optimization steps are discussed.

### *5.2.1 Method limitations and recommendations*

The method chosen for the experiment has a few steps that could be changed or optimized to increase the reliability of the results. In all of the images a lot of background noise is visible and especially from the actin staining it was problematic analyzing the images due to the high background noise. It is possible that the high amount of background noise blocks out information about less reactive astrocytes, causing limitations of the analysis. The cause for the high

background noise can be due to the following suggestions: too thick gel layer, meaning that the cells in the other planes will have an impact on the image or due to over-staining; caused by too high dye dilutions, insufficient washing of the gels or non-specific binding of the staining. These are all problems that can be solved by optimizing the staining protocol and some suggestions of steps to improve are proposed in the following paragraph.

In each well 50 µl of the gel was added causing a thickness of 1.5 mm, which will cause a lot of noise from planes out of focus in the plane being analyzed (compare it to the height of the microfluidic channel that is 375 µm). This is simply avoided by adjusting the thickness of the gel. Especially when a higher cell concentration is used a thinner gel is preferable. When it comes to over-staining it can usually be seen by the background noise. In our case we had a control for the antibody staining, where only the secondary antibody was added together with the staining for actin. The average intensity from these images is about 6% of the total intensity, which is relatively high. Although in this experiment the recommended dilutions (from manufacturer) were applied, it is always better to optimize the staining dilutions for the specific application, as the results can differ between systems. Especially for staining of cells inside a gel, optimization of the protocol is recommended as the incubation and washing steps need to be prolonged due to slower flow through the gel. Other recommendations to remove background noise are adding extra washing steps or prolonging the already existing ones as the washing occurs through diffusion which will take a longer time. Another idea could be to use another blocking buffer in order to prevent non-specific binding, and since in our system we are using a secondary antibody from goat, adding a goat serum could be a possible option for decreasing the non-specific staining.

The background noise could be the reason for the low percentage of GFAP positive cells detectable, shown by Graph 1. However, this does not explain the reason for the low GFAP expression in the 2D control where there are very low levels of background noise, shown in Figure 24F. From the hypothesis a high GFAP expression should be distinguished from the astrocytes cultured in 2D, due to an increased reactivity. Furthermore, non-reactive astrocytes also express GFAP and therefore a higher percentage of cells expressing GFAP were expected. In literature it has been reported that there are several different types of astrocytes present in the brain and that not all of these express GFAP [93]. However, from manufacturer's notes 95% of the astrocytes that were used for this experiment express GFAP (ScienCell). Another possible reason for the absence of GFAP could be loss of phenotype of the cell culture. In section 3.3.2 it is mentioned that the doubling capacity of the cells are limited. There is a possibility that a high

passage number (for this experiment passage 8 was used) of the cells may have altered their phenotype, causing the absence of GFAP expression. It is always recommended to use a low passage number, especially when working with primary cells.

All images were analyzed using ImageJ and during the analysis certain choices were made. In the method chosen a lot of the analysis was done manually, such as counting the cells and drawing out the cell shape for intensity measurements. By performing the analysis manually human errors can be included as well as differences between the analysis of different cells. An option is to create an image analysis program to standardize the method and ensure fewer differences in analysis between cells. A problem with an image analysis program is that the images used are taken in a gel, causing cells in other planes to influence the analysis. Such a program needs to be capable of distinguishing between cells in plane and out of plane. In a try to manually remove cells out of plane from the analysis, a threshold was set for the intensity of the nucleus and only cells with a visible nucleus were analyzed. This meant that even if a cell was clearly visible with actin and GFAP staining it would not be used for analysis if the cell nucleus was not visible. A clear example of this situation is shown in Figure 27, where a visible cell without a corresponding nucleus is shown, meaning that for this analysis it was not included.

One of the main goals with the image analysis was to choose a method that is as objective as possible in order to not be biased by our expectations, which unfortunately complicated the image analysis. When imaging in gels the cells will be spread out throughout the planes making it problematic to visualize the complete morphology of the cells. The cells will also be spread out in the different planes, limiting the amount of cells to analyze if the plane is fixed, like in the method chosen in this experiment. To ensure a higher cell density in the planes the cell concentration could be increased, although then there will be more background noise as well that may affect the results.

One solution to the problems obtained with the current method is imaging with a confocal microscope instead of a fluorescent microscope. With a confocal microscope 3D images are obtained by imaging the different planes and reconstructing the 3D volume. This has the advantage of removing the background noise caused by cells in other planes, but also the possibility to see the complete morphology of the cells, as the processes are spread out through different planes. A dilemma with using a confocal microscope is that the focus depth is limited and in order to receive high quality images there are limitations

on the thickness of the culture device. An alternative way of analyzing GFAP expression is through Western blot, a technique used to detect and measure proteins, which has been used in literature to evaluate GFAP expression levels in astrocytes [94-95]. Even though the information about the expression on a single cell level will be lost, more precise results of the total GFAP expression will be obtained.

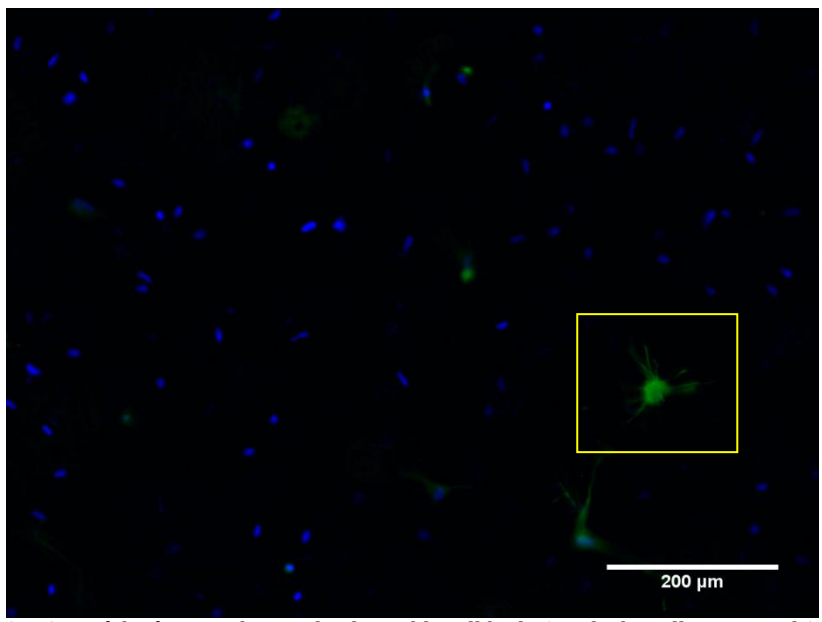


**Figure 27.** One of the frames where a clearly visible cell body (inside the yellow rectangle) is seen through expression of GFAP, although there is no visible cell nucleus corresponding to the cell body. Therefore, the cell was not used for analysis. Image taken with GFP and DAPI filter cubes.

## 5.3 Conclusion

In this experiment the influence of culture environment on astrocyte reactivity and morphology was evaluated. Astrocytes were cultured in different combinations of collagen type I and HA hydrogels and compared to conditions reported to induce a higher reactivity, such as a collagen type I gel and a 2D surface. In the results obtained from the image analysis of GFAP expression less than 10% of cells in all conditions expressed detectable levels of GFAP and the on average lowest GFAP expression were found in the 4 mg/ml collagen type I and the 3 mg/ml collagen type I and 1 mg/ml HA hydrogels. From the morphology data a majority of cells analyzed exhibit a star-shaped morphology, although the amount of cells used for the analysis were too few to make it statistically relevant.

Due to the limitations of the used method the choice of gel combination used for the following experiment will also be influenced by the results from the article by Placone et.al [77]. Therefore, the gel concentration of 3 mg/ml collagen type I and 1 mg/ml HA was chosen for further use.

# 6 Experiment 3: Co-culture in a BBB-chip

The main component of the BBB is a monolayer of endothelial cells that makes up the physical barrier between brain and circulatory system, making it the main target for BBB modeling. However, astrocytes that are in close contact with the barrier through their endfeet are hypothesized to play a role in inducing and regulating BBB-specific properties of the brain endothelial cells. To evaluate the influence of astrocytes on endothelial cells a co-culture system inside a microfluidic chip was established where the barrier tightness was assessed through TEER measurements. It was expected to see a slight increase in TEER between chips containing a co-culture of endothelial cells and astrocytes compared to chips seeded with only endothelial cells.

## 6.1 Materials and methods

In the experiment a total of 15 chips for four conditions were tested. The different conditions and number of chips for each condition is shown in Table 3. The design of the PDMS chip (described in section 3.1) used for all conditions contains a top and bottom channel aligned perpendicular to each other, creating a crossing of the channels in the middle of the chip with a polycarbonate membrane separating the channels (for protocol see appendix A. Chip fabrication).

**Table 3.** Summary of the four different conditions used in the experiment. For condition 1 six chips were used where endothelial cells and astrocytes in a hydrogel were present. In condition 2 three chips were used with astrocytes in a hydrogel present, while endothelial cells were absent. In condition 3 three chips were used with endothelial and a hydrogel, however there were no astrocytes incorporated in the gel. In condition 4 three chips were filled with endothelial cells while the hydrogel and astrocytes were absent.

| Condition | 1 | | | | | | 2 | | | 3 | | | 4 | | |
|---|---|---|---|---|---|---|---|---|---|---|---|---|---|---|---|
| Endothelial cells | + | | | | | | - | | | + | | | + | | |
| Astrocytes | + | | | | | | + | | | - | | | - | | |
| Hydrogel | + | | | | | | + | | | + | | | - | | |
| Chip number | 1 | 2 | 3 | 4 | 5 | 6 | 7 | 8 | 9 | 10 | 11 | 12 | 13 | 14 | 15 |

After chip assembly the channel surfaces were functionalized with APTES and GA according to the protocol described in section 4.1. The chips were kept in the oven at 60°C for 2 h and afterwards coated with a 10 µg/ml solution of collagen type I and incubated at 37°C for 30 min. The pre-coating of collagen was added to ensure the stability of the surface treatment over a longer storing time. The

collagen solution was aspirated from the channels and the chips were stored at 60°C over night.

Electrodes were cut into pieces from a platinum wire with a diameter of 200 µm (Alfa Aesar). After aligning the electrodes in the middle of the channels, UV-curable glue was added to the opening of the electrode channel (Norland Optical Adhesive 81, NOA81). Through capillary forces the glue entered the channel and when cured with ultraviolet (UV) light (350 $mW/cm^2$ for 5 s), it fixated the electrode in the channel. Chip and electrodes were attached to the bottom of a plastic dish with a 2-component epoxy adhesive (Loctite M-31 CL Hysol, Henkel) and baked in the oven at 40°C over the weekend. An image of a fully assembled chip can be seen in Figure 28.

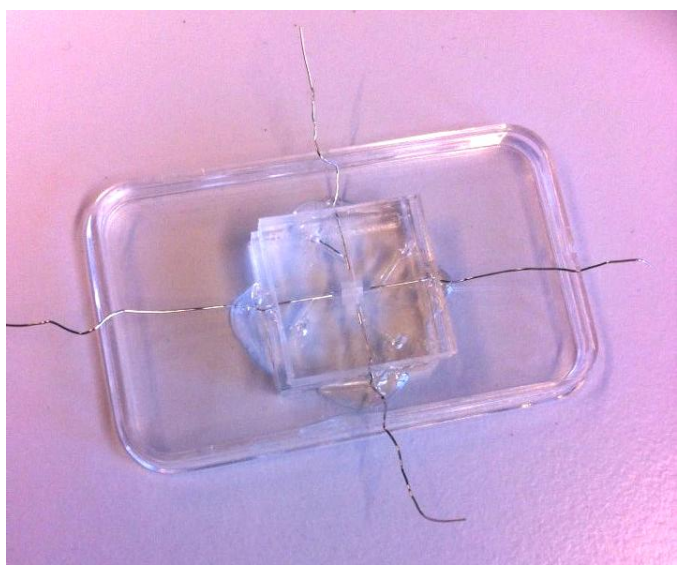

**Figure 28.** Image of the assembled two-compartment chip containing two channels aligned perpendicular to each other. The two channels are separated by a membrane and in each channel two electrodes are introduced on each side of the membrane. The chip is glued to a plastic dish.

The chips were kept at 4°C for 2 h prior to adding cells. 10X PBS, 1M NaOH and astrocyte medium were added to Eppendorf tubes and kept cold. Astrocytes (passage 4) were detached from their flasks and cell concentration was counted. Collagen type I (3 mg/ml) was added to the cold Eppendorf tubes, HA (1 mg/ml) and PEGDA were mixed together (through pipetting) in a separate tube and directly afterwards pipetted into the Eppendorfs. Lastly, the cells suspended in AM were added to the gel ($1.0 \cdot 10^6$ cells/ml) and directly after thorough mixing through pipetting, the liquid gel was added to the bottom channels (see appendix

A. Hydrogels). The chips were incubated at 37°C for 30 min to make sure the hydrogel had gelled prior to adding AM and directly afterwards the top channel was coated with fibronectin at a concentration of 40 µg/ml. Chips were incubated for 1 h and afterwards flushed with EGM-2.

TEER measurements of the blank chips were performed prior to seeding the endothelial cells in the chips (see section 2.2.3 about TEER measurements). In order to seed the endothelial cells (passage 34) in the chips they were detached from the flasks and pipetted into the top channel at a concentration of $5.0 \cdot 10^6$ cells/ml. The chips were kept in the incubator for 1.5 h before flushing the channel with EGM-2. Every morning and afternoon medium for the bottom channel (AM) and top channel (EGM-2) was changed and approximately 2 h after the medium was changed in the morning, TEER measurements were carried out.

On the fifth and last day of the experiment the cells were fixated and stored in 1X PBS at 4°C over the weekend. The staining protocol described in appendix A. Staining of cells was performed using NucBlue and ActinGreen.

## 6.2 Results and discussion

TEER series for the 15 chips showing the membrane resistance values for the five days duration of the experiment are shown in Graph 4-7, in which the results have been summarized depending on condition. To obtain the TEER value the resistance obtained on day 0 needs to be subtracted from the values of the following days.

In Graph 4 the TEER values from the co-culture systems are summarized. In a typical TEER measurement a low resistance is measured on the blank chip (day 0) and after the addition of endothelial cells an increase in resistance is expected. This increase is due to the formation of the cell monolayer and the tight junctions between the cells, which commonly takes a couple of days. Only in chip 1 a typical TEER series is measured, while in the other chips the resistance either stays more or less constant (chip 3-5) or is even decreased (chip 1). In chip 2 a negative resistance is measured on day 0, however on the other days of the experiment a positive value is measured.

In Graph 5 the TEER series of condition 2 has been summarized. In these chips no endothelial cells were added and therefore it is not expected to see an increase in TEER values. In one chip the resistance stays constant throughout the experiment, while in the other two chips differences in resistance can be seen for the two first days, and afterwards they as well become constant. Worth noting is

that on day 0, when a blank measurement was carried out, a very high resistance was measured in chip 9.

In condition 3 and 4 endothelial cells were added in the top channel while in condition 3 only the hydrogel was added and in condition 4 the bottom channel was only filled with medium. In both Graph 6 and 7 either a decrease or increase in resistance can be seen in most of the chips between day 0 and 1, and for the remaining days only small variations in resistance are measured.

From the TEER series only in one of the chips a characteristic TEER measurement is seen. In most of the other chips a constant TEER at a low value is shown from day 1 or 2, indicating that there is no monolayer of endothelial cells. The large variation in TEER values typically seen between the first days can be due to disturbances or changes in the system. From images taken at the same time as the TEER measurements, on day 0 large bubbles either directly in contact with the electrodes or blocking the channel are seen (Figure 29 and 30). These bubbles may be the cause for the atypical resistance values seen the first days. In three of the chips (chip 2, 10 and 13) a negative resistance is obtained on the first day of measurements. This is most likely due to bubbles either blocking or covering both electrodes in a channel, causing a high resistance across the channel. From equation 10 (see section 3.4.2) it can be understood how a high resistance along one or both of the channels can cause the calculations of the membrane resistance to become negative. However, after one or two days the bubbles had typically disappeared, which may be the explanation for the large variations between the days. Other factors that may influence the TEER measurement is if there is any damage to the membrane or the pores are partly blocked, which can typically be distinguished by higher resistance values that causes a constant offset in the measurements.

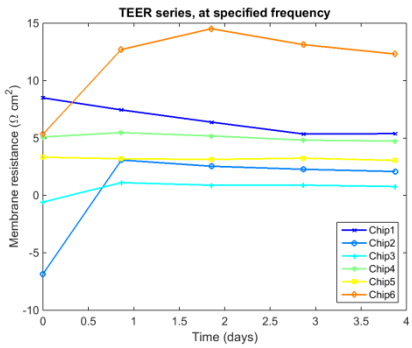


**Graph 4**. A graph showing the TEER series at 10 kHz for chip 1-6. In the graph the membrane resistance ($\Omega$*cm$^2$) over time (days) is shown for the chips.. In chip 3,4 and 5 a nearly constant membrane resistance for all measurements were obtained. In chip 1 the membrane resistance decreased with time until the last two days when it was constant. In chip 2 the membrane resistance is negative on day 0 and on day 1 it has increased to above 0 $\Omega$*cm$^2$, however for the days to follow the value is constant. In chip 3 an increase can be seen in membrane resistance from day 0 to day 2, and in the following days a small decrease is measured.

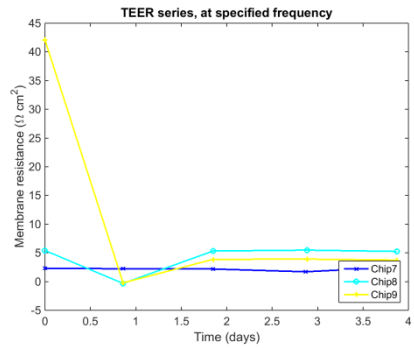


**Graph 5.** A graph showing the TEER series at 10 kHz for chip 7-9. In the graph the membrane resistance ($\Omega$*cm$^2$) over time (days) is shown for the chips. In chip 7 a low membrane resistance was constant over the five days. In chip 8 the resistance decreased from day 0 to day 1, however on day 2 it went back to the same resistance as day 0 and stayed constant for the rest of the experiment. In chip 9 a large resistance was measured on day 0 which by day 1 had decreased to close to 0 $\Omega$*cm$^2$. At day 2 the resistance had increased to approximately 5 $\Omega$*cm$^2$, and stayed constant at this value for the days to follow.

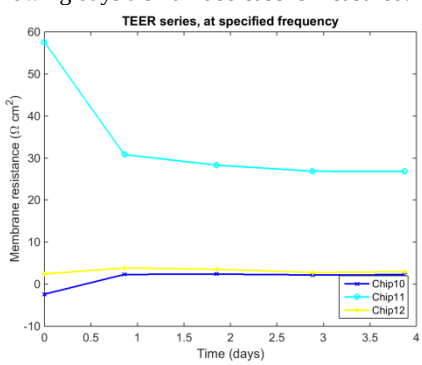


**Graph 6.** A graph showing the TEER series at 10 kHz for chip 10-12. In the graph the membrane resistance ($\Omega$*cm$^2$) over time (days) is shown for the chips. In chip 10 and 12 the resistance stayed close to 0 $\Omega$*cm$^2$ for the full duration of the experiment. In chip 11 a high resistance of 60 $\Omega$*cm$^2$ was measured on day 0 and on day 1 it was decreased to half that value, where it also stayed constant until the last day.

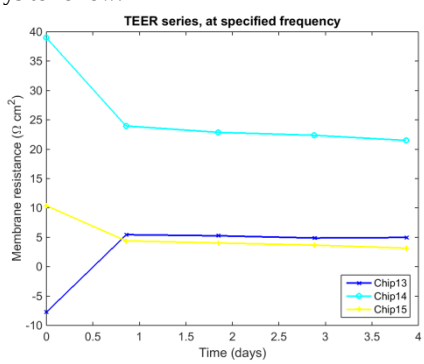


**Graph 7.** A graph showing the TEER series at 10 kHz for chip 13-15. In the graph the membrane resistance ($\Omega$*cm$^2$) over time (days) is shown for the chips. In chip 13 the membrane resistance started at a negative value on day 0. For day 1-4 the resistance was constant at approximately 5 $\Omega$*cm$^2$. In chip 14 a high resistance was measured on day 0, and for the remaining days it kept on decreasing. In chip 15 a high membrane resistance was first measured and after a decrease between day 0 and 1 the value stayed more or less constant.

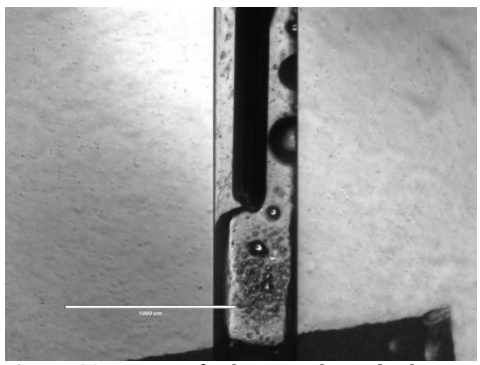

**Figure 29.** Image of a bottom channel where a large bubble has been incorporated in the gel. Taken with phase contrast microscopy with a scale bar of 1000 µm.

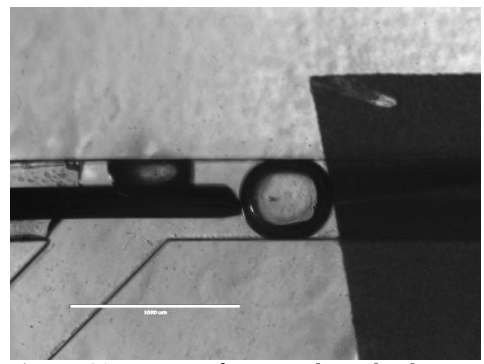

**Figure 30.** Image of a top channel where a bubble has been incorporated in the fluid-filled channel. Taken with phase contrast microscopy with a scale bar of 1000 µm.

### *6.2.1 Top channel*

The TEER series obtained indicated that no monolayer of endothelial cells had been formed. From images taken with the phase contrast microscope it is shown that viable endothelial cells were present in the channels on day 1 after seeding. After this day a decrease in viability is observable each day, and by the end of the experiment the layer of endothelial cells in the chips was discontinuous and most cells had a rounded morphology, indicating that the cells were dead. The decreased viability can be seen by comparing images taken of a chip at day 1 and day 4 (Figure 31 and 32).

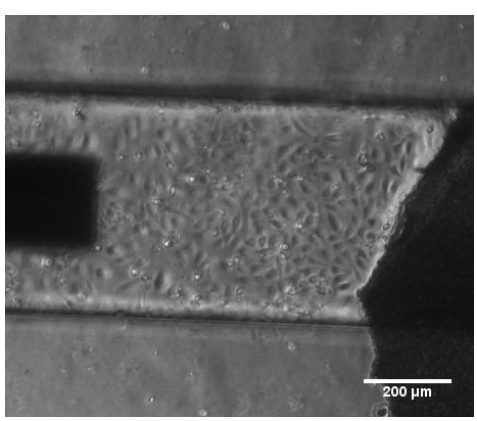


**Figure 31.** Image of the top channel in chip 2 on day 2 where endothelial cells are visible. Taken with phase contrast microscopy with a scale bar of 200 µm.

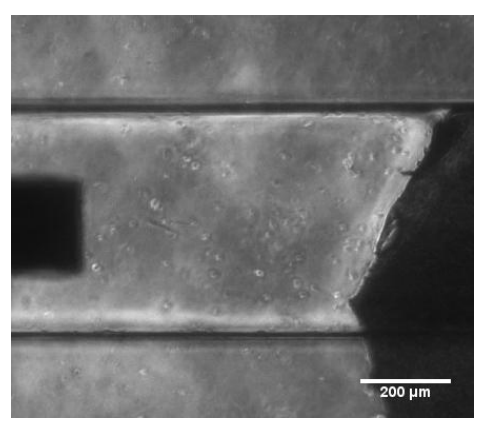


**Figure 32.** Image of the same top channel as seen in Figure 31 on day 4 with few cells visible. Taken with phase contrast microscopy with a scale bar of 200 µm.

The same behavior was observed in all chips except for one, where endothelial cells grown on the membrane created a monolayer. For chip 6 a characteristic TEER measurement was obtained and the monolayer is visible with fluorescent staining for nucleus and actin (see Figure 33). Worth noting is that in this chip it can be seen that on the surface of the channel next to the membrane very few viable cells are present.

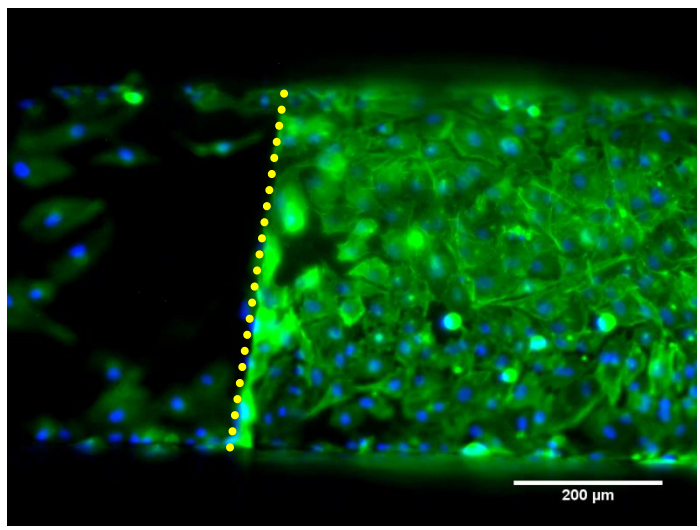


**Figure 33.** Image of the top channel showing a part of the channel and the membrane in chip 6. A monolayer of endothelial cells is seen grown on the membrane. Yellow dots mark the beginning of the membrane (moving from left to right). Stained with ActinGreen and NucBlue and images taken with fluorescent microscope using GFP and DAPI filter cubes. Scale bar is 200 µm.

The protocol used for chip fabrication, seeding of endothelial cells and TEER measurements is a standardized protocol used several other times without complications [61]. Therefore it would seem most likely that the reason for the low viability is due to one of the newly added protocols or one of the materials used. In the discussion to follow some of the possible causes are brought up and discussed.

One source of variation between experiments is the cells. A different passage number can have an effect on the cell function. Other factors which may influence the viability of the cells are infections, such as mycoplasma, and air bubbles in the channels. For this experiment the endothelial cells were passaged into three flasks the weekend before the experiment, where two flasks were used for this experiment and one flask for another experiment, independent of the one presented here. The cells in the other experiment did not show any abnormal behavior and a high viability. This indicates that the problem may instead be due

to the interaction between cells and device. The main material that the cells are in contact with is the PDMS and one of the reasons for using PDMS in BioMEMS is its biocompatibility. However, uncured PDMS is capable of diffusing through the chip and enter the culture channel, which may influence the cells. The curing process of PDMS is temperature and time dependent and despite a proper curing protocol it is hard to ensure the absence of uncured PDMS [96]. The chips used for this experiment were stored either for one or two weeks prior to use at room temperature and at 40°C for 72 h before adding cells to the chips. Due to the long storing times and exposure to high temperatures, only a low amount of uncured PDMS should be present, although this has not been proven. Other materials of the chip that were in contact with the cells are the electrode parts, consisting of platinum electrodes and UV-curable glue. Platinum is a metal with high biocompatibility and has been used in several biomedical applications [97]. The glue is a polymer that cross-links when exposed to UV and has been reported to have a high biocompatibility [98]. However, for the chips used in this experiment the glue looked damaged after having been stored in the oven over the weekend. This appearance had been seen in a previous smaller scale experiment, where the same chip design treated with APTES and GA was stored in a desiccator over the weekend. Comparison of a channel containing the glue in its normal state and the damaged glue is shown in Figure 34 and 35.

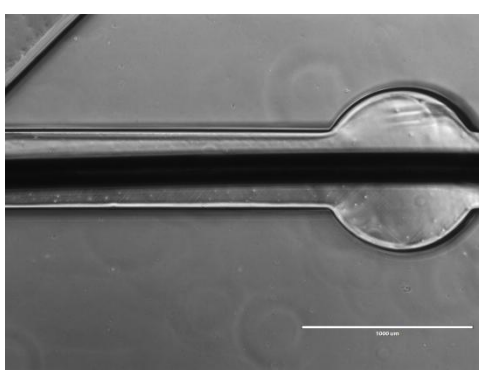

**Figure 34.** Image of an electrode channel containing an electrode and UV-curable glue. The typical appearance of the glue is shown Chip without surface treatment stored in room temperature. Taken with phase contrast microscopy and scale bar is 1000 µm.

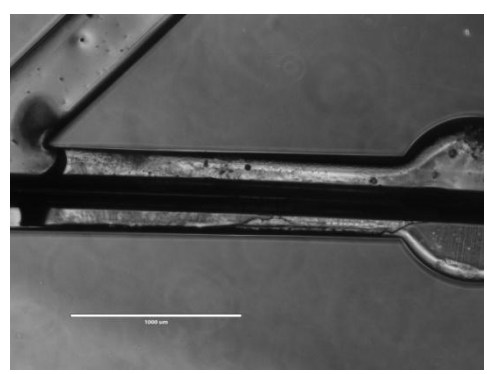

**Figure 35.** Image of an electrode channel containing an electrode and UV-curable glue. The atypical appearance of the glue is shown. Chip with surface treatment and stored in an oven. Taken with phase contrast microscopy and scale bar is 1000 µm.

The reason for why the glue had changed in appearance has not been determined; however, a couple of possible reasons will be mentioned. The glue used for this experiment, as well as for the smaller experiment mentioned above, was past its

expiration date and there is a risk that the exposure time used was not enough to cure the glue completely. Another possibility could be that the interaction between the surface functionalization and the glue has an influence on the curing of the glue. This appearance of the glue, seen in Figure 35, has only been seen after the two protocols were combined. As the surface treatment is carried out before the electrodes are added it may have an effect on the curing of the polymer.

Another step added to the standard culture protocol for endothelium on chips is the surface functionalization with APTES and GA. As growing cells directly on the treated surface would cause harm to the cells, the APTES and GA treated surface was coated with collagen type I and fibronectin prior to seeding, which should be enough to create a biocompatible surface for the cells to attach to according to literature [70].

Without further experiments it is not possible to determine the exact reason for the decreased viability of the endothelial cells.

### *6.2.2 Bottom channel*

Apart from the endothelial cells in the top channel, astrocytes were seeded in a hydrogel in the bottom channel. In most chips the gels had detached partly or completely from the walls by the end of the experiment. The cell density was low and in some gels the cells showed a rounded morphology, indicating a decreased viability of the astrocytes inside the gel. In case of gel detachment the largest detachment was in general close to the inlet where the medium was refreshed. Inside the gels few viable astrocytes with the characteristic star-shaped morphology could be found and instead most cells had an elongated morphology.

In the first experiment different surface treatments to avoid gel detachment from the walls were evaluated, and the treatment with APTES and GA was chosen due to its high interaction with the hydrogel. However, in this experiment most of the gels had detached by the last day of the experiment, despite surface functionalization. Although the cause for this is not certain, there are three things worth mentioning that may have had an influence. Firstly, the largest degree of detachment was in almost all cases close to the inlet where the medium was refreshed. Medium refreshing was carried out by first adding a pipette tip of 150 µl to the inlet and afterwards a pipette tip with 100 µl to the outlet. Especially when the first pipette tip is inserted it will cause high forces on the gel which could cause the detachment in the case of an already instable gel. Secondly, in the gels where no astrocytes were present gel detachment could also be seen, however it tended to be smaller than in the gels containing astrocytes. This indicates that

forces exerted by cells on the gel matrix contribute to the detachment. Therefore, a more stable gel, for example through higher gel concentration, could be a solution for decreased detachment. Thirdly, at day 0, in almost all the chips with gels, bubbles were incorporated in the gels in proximity to the electrodes (see Figure 36 and 37). The incorporation of air bubbles in the gel can either have occurred during the mixing of all gel components through pipetting, or after adding the gel to the chip. The gels were made in four different tubes and all of them were carefully mixed in order to ensure that no bubbles would be incorporated. The fact that bubbles are seen in all chips makes it unlikely that the bubbles were created during the mixing. Also, in other experiments using the same method for mixing but chips without electrodes, there were rarely any problems with bubbles. For this reason it is thought that either the electrode integration or the electrode in itself is the cause for the air bubbles. The UV-curable glue used to attach the electrodes to the channels cross-links when exposed to UV. This cross-linking will cause it to shrink, causing a gap between the channel wall and the glue. This was visualized in a video where the curing procedure was filmed, where it is possible to see the glue detaching from the wall of the channel when being cured. This could be a possible source of the air bubbles. Another possibility is the application of a potential during the TEER measurement, causing electrolysis of water. Electrolysis is the process of splitting water molecules into hydrogen and oxygen gas by applying an electrical potential. As in theory a potential of 1.2 V is needed for electrolysis while in the TEER measurements a potential of 0.3 V is applied to the electrodes, it is not likely that this is the source of the bubbles in this system [99]. After one or two days the bubbles break, causing the gel to be detached from the wall in those spots. When medium-filled pipette tips are added the detached part will be the preferred path for the medium to flow, causing higher forces on the gel that is still attached to the wall, accelerating the detachment process.

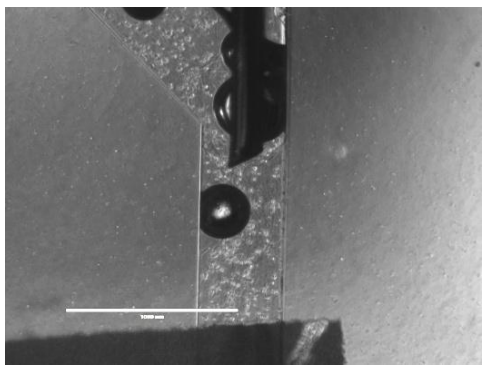

**Figure 36.** Image of chip 5 close to the electrode in the bottom channel. Several bubbles are incorporated in the gel, close to the electrode.

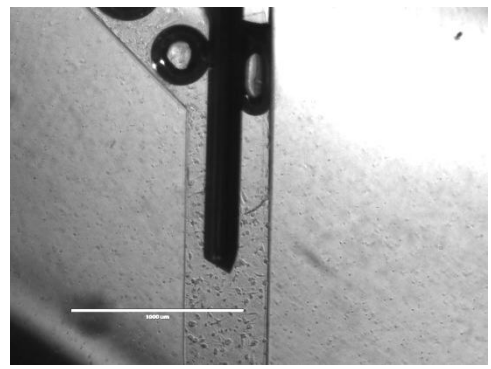

**Figure 37.** Image of chip 3 close to the electrode in the bottom channel. Two bubbles are incorporated in the gel, close to the electrode.

Apart for the complications with gel detachment the viability of the astrocytes in the gel varies between chips. In some chips a good viability is seen (Figure 38), while in other chips there are no visible cells at all. This could be related to problem of the decreased number of endothelial cells, although their different culture protocols inside the chip will make some of the alternatives given in the discussion about the viability of the endothelial cells less likely. The astrocytes are cultured inside a gel, causing them to not be in contact with surfaces of the channel. In parts of the channels where the gel has detached the astrocytes are growing on the channel with a high viability (see Figure 39). This could be because parts of the gel are covering the surface, allowing the astrocytes to grow on it without being in any contact with the surface functionalization. Another possibility brought up in the previous discussion was the electrode integration. Since electrodes are inserted in the bottom channel, this could be a possible cause for the decreased astrocyte viability. However, once again it needs to be mentioned that the cause cannot be determined without further investigation.

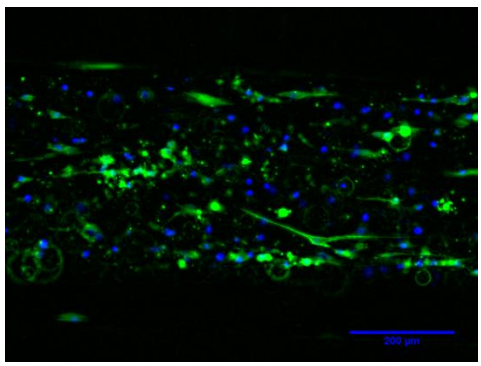

**Figure 38.** Image of the bottom channel showing astrocytes spread out in a gel. Taken with fluorescent microscope using DAPI and GFP filter cubes. Scale bar is 200 µm.

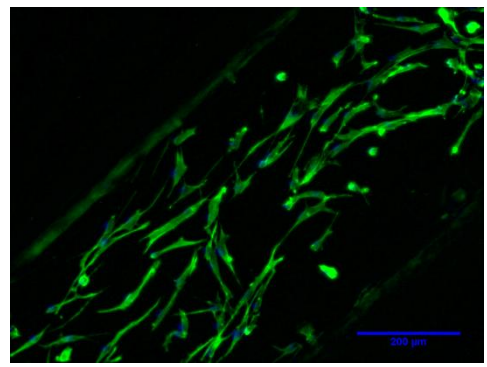

**Figure 39.** Image of the bottom channel where the hydrogel has been detached. Astrocytes grown on the bottom of the channel can be seen (all in focus). Taken with fluorescent microscope using DAPI and GFP filter cubes. Scale bar is 200 µm.

## 6.3 Conclusion

In the third experiment endothelial cells and astrocytes seeded in a hydrogel where co-cultured inside a BBB-chip to evaluate the influence of astrocytes on the barrier. From the results obtained it is hard to draw any conclusions about the effects of astrocytes on barrier tightness as there were no continuous monolayers of endothelial cells. However, there are several examples of similar co-culture systems in literature and a discussion about co-culturing systems can be read in section 7.3. Instead, what can be concluded from this experiment is that the current chip design may not be optimal for the incorporation of a hydrogel to establish a co-culture system.

# 7 Discussion

In this section three topics will be discussed in further detail. First of all, the chip design and its suitability for hydrogel incorporation will be discussed. In the second section a summary of the importance of the culturing environment on astrocytes will be given, that is based both on literature and results from the experiment. In the third and final section the effects of co-culturing endothelial cells and astrocytes based on literature will be discussed.

## 7.1 Chip design

In the final experiment the goal was to co-culture endothelial cells and astrocytes seeded in a hydrogel inside the BBB-chip that was previously developed.

The BBB-chip had been optimized for growing a monolayer of endothelial cells exposed to shear stresses and measuring the TEER across the barrier. With the bottom channel previously being used for medium, the potential of incorporating astrocytes within this channel was promising. This would allow for the two cell types to be cultured in proximity to each other, only separated by a membrane. To culture astrocytes in the bottom channel they could either be grown directly on the surface of the channel or inside a hydrogel. Since astrocytes cultured in 2D are reported to have a less physiologically relevant behavior compared to cells cultured in 3D, it was decided to incorporate the cells in a hydrogel [100].

Due to the hydrophobic nature of PDMS, interactions between hydrogel and channel walls are low which may cause the hydrogel to detach from the channel. With the addition of cells exerting forces on the hydrogel structure the risk increases. Therefore a strong interaction between the hydrogel and channel walls was desired and by functionalizing the PDMS surface with APTES and GA this strong interaction was achieved. However, the protocol for the surface treatment is more extensive than other commonly used treatments for increased PDMS functionalization and it was also discussed earlier in this report about the compatibility between the surface treatment and the UV-curable glue (see section 6.2.1). There are some options to be considered with the current protocols. To achieve strong enough interactions without using the APTES and GA treatment the gel composition or cross-linking can be increased and also another chip material that is more hydrophilic could be considered. Another option is to change the chip design in order to decrease the forces applied to the gel structure, making it more suitable for the incorporation of a hydrogel.

Fluidic flow through a gel is a tedious process and depends on the composition of the gel. By adding the fluid with a higher pressure the flow rate can be increased. This will also mean that the gel will be exposed to higher forces, creating a greater risk for gel detachment. Another argument against increased flow rate is its influence on the cells. The second experiment presented in this report was first carried out in microfluidic chips, where the flow rate of the medium had been increased from experiment one to two. By the end of the experiment few viable cells with processes were visible, and it was hypothesized that the cause was the high medium flow in combination with the low cell concentration, due to the forces exerted on the cells in combination with low signaling between cells (both due to the flow and low cell concentration). From literature examples of different chip designs for hydrogel incorporation in a microfluidic chip can be found. One example is to have separate hydrogel and medium channels, where the medium will reach the cells inside the hydrogel through diffusion [9]. In another device a hydrogel chamber containing an array of micro-pillars is connected to two microfluidic channels. The micro-pillars are used as a physical support for the hydrogels, allowing the use of lower gel concentrations and softer gels [101]. Even though it is not the optimal design for the incorporation of a hydrogel, gel attachment was achieved in both experiment one and two after surface functionalization with APTES and GA.

In the third experiment though, unforeseen problems with gel detachment occurred.

In the first two experiments a single-channel PDMS chip connected to a PDMS-coated glass cover slip was used. For most of these chips treated with APTES and GA the interactions between channel walls and hydrogel were strong which led to high attachment. In the third experiment, however, in the edges of the channels electrodes had been integrated by fixating platinum electrodes into a separate channel with glue that cross-links when exposed to UV. In these chips air bubbles were seen in almost all the gels and the gel had detached close to the inlet, outlet and the electrodes in several chips. The detachment of the gel is most likely due to the bubbles, that after breaking will cause detachment of the gel from the wall, or that the channels are not properly filled with the gel due to the electrodes. The cause for the formation of the bubbles is not yet determined, although there are a few possibilities that have been considered. When the UV-curable glue is cross-linked, it detaches from the channel wall leaving a small gap that will be air-filled prior to adding the gel. Although it is still not certain whether this is the source of the air bubbles, the electrode compartment seems to be the most likely cause for the problems in incorporating hydrogels in the bottom channel of the chip. Further

investigations into what is causing the air bubbles is needed before a co-culture system can be established.

The co-culture system in the current design is established by culturing the cells in two channels separated by a polycarbonate membrane with a pore size of 4 µm and a thickness of 10 µm. The membrane is added for structural support of the endothelial cells that are in need of a surface to adhere to. In the co-culturing system this membrane will create a distance between the two cell types, causing low interaction between them. Direct contact between the two cell types would more resemble the *in vivo* situation, although for the current chip design the feasibility of such a direct co-culture system is low. However, such a system does not only depend on the chip design, but also on the structure of the hydrogel. Endothelial cells exert high forces on the surface that they are grown on, and to avoid gel contraction the gel needs to be strong enough or have enough support to withstand those forces.

## 7.2 Culturing condition's impact on astrocytes

The effect of the environment on cultured astrocytes has not been given a lot of attention. There are some reports on the effect of culturing astrocytes in 2D compared to 3D when it comes to reactivity [100], but the effect of culturing the cell type in different gels is not very extensively investigated.

The most commonly used hydrogel for culturing astrocytes is a collagen type I gel. However, collagen type I is only present at very low levels in the healthy ECM of the brain and especially for primary cells this may have an effect on their molecular expression as well as their functions. In the article by Payne and Huang [102] it is claimed that when there is cancerous tissue in the brain, elevated levels of collagen type I can be found in the brain. In that case the presence of collagen type I is a sign of injury to the brain, which in theory should lead to an increased reactivity of the astrocytes. In other studies such it has been shown that the addition of HA, which is one of the most abundant components of the ECM in the healthy brain, can decrease the glial scar formation that is connected with astrocyte reactivity [103]. Therefore the addition of HA would make the hydrogel resemble the natural ECM more and cause a lower reactivity of the cells, as seen in the article by Placone et.al. [77].

In the results obtained from the experiment presented in this report a higher GFAP expression could be seen in the conditions with a higher polymer concentration. However, no statistically significant difference could be seen for the GFAP expression between cells cultured in the 4 mg/ml collagen type I and 3

mg/ml collagen type I and 1 mg/ml HA hydrogels. In the article by Partyka et.al [92] they compared astrocytes grown in a collagen type I and a mixture of collagen type I, HA and Matrigel hydrogel. In the images presented in the paper there is a very low degree of GFAP expression in both the collagen and the collagen and HA gel and there is no visible differences in expression levels between the gels. It is not until the addition of EGM to the astrocytes that an increased GFAP expression is visible. However, they do not present a comparison of reactivity and morphology of astrocytes between the two gels. The results indicate that the addition of HA to the hydrogel is not the factor that influences the reactivity of the cells the most. The trend that can be seen in this study, which has also been reported in the article by Placone et al [77], is that the mechanical properties, such as stiffness and relaxation rate, of the gel will also have an influence on the reactivity. A higher total polymer concentration will cause a stiffer gel, and there are indications that the stiffness of the gel may be an important factor for astrocyte reactivity and morphology, as well as the relaxation rate. Complementary tests of the mechanical properties of the gels used to culture astrocytes could provide interesting and useful information in future studies.

In this study the ratio GFAP positive cells was also very low. One likely reason for the low degree of cells visibly expressing GFAP is that there is a very low degree of expression in the cells and that the background noise is too high for these lower levels of expression to be detected. However, from the 2D condition, where a very low background noise was measured, a low ratio of GFAP expressing cells was detected, possibly due to loss of phenotype. Further investigation is needed to decide the cause for the few GFAP positive cells. However, since the amount of data obtained from this study, both on GFAP expression and morphology, is not enough to be statistically relevant, no conclusion can be drawn about the effect of culturing environment on astrocytes.

## 7.3 Co-cultures

While a monolayer of endothelial cells is the component that builds up the barrier between brain and circulatory system, the barrier is strongly influenced by its surrounding environment. When modeling the BBB with only endothelial cells a lot of information is lost, and therefore co-cultures with other components of the NVU is becoming more commonly used. Astrocytes are one of the cell types that have been given a great deal of attention and interest due to their capability to induce BBB-specific properties of the endothelial cells, and there are several studies on co-cultures of endothelial cells and astrocytes. However, the extent of

astrocyte influence on barrier properties differs between studies, and also between cell lines.

For the experiments presented in this report the immortalized cell line hCMEC/D3 was used. Since the cell line is obtained from human brains, signaling pathways, protein expression and metabolism are the same. The main problem with this cell line is the low barrier tightness, causing a higher permeability of smaller molecules across the barrier. Due to its other promising qualities for BBB research, possibilities to increase the tightness of this cell line have been investigated. Two methods that have been especially looked into are the application of shear stress to the cells by applying a flow, and co-culturing the cell line with other cells known to induce BBB properties, such as astrocytes and pericytes. In static models where hCMEC/D3 are co-cultured with astrocytes a small increase in TEER values can be observed, while when co-cultured with pericytes no significant increase is shown. What seems to have a larger influence on the hCMEC/D3 cell line is the addition of shear stresses to the cells, at least when looking at TEER values [49, 104].

Therefore, the question arises about the need for co-culture systems when working with the hCMEC/D3 cell line, if there is only a small increase in barrier tightness. One thing to keep in mind is that astrocytes not only induce BBB properties, but may also be involved in the disruption of the BBB during damage to the brain [105]. The reactive state of astrocytes leads to functional and molecular changes of the cells, which may influence the BBB. In a study by Hawkins et.al [12] co-culturing endothelial cells and astrocytes in a Transwell system did not result in a statistically significant increase of the TEER value compared to culturing only endothelial cells, both when astrocytes were cultured in 2D and 3D. However, when adding an agent that causes increased reactivity of astrocytes, a decreased TEER was measured compared to when the agent was added to the system containing only endothelial cells.

Although the importance of astrocyte reactivity on the BBB has not been given a lot of attention yet, from these preliminary studies it appears as if the astrocytes play an important part for the barrier integrity, both in health and disease.

## 7.4 Ethical reflection

One of the largest dilemmas today is that new drugs fail in a late stage of development, as there are few testing models for earlier stages of development capable of faithfully replicating the complex structure and environment of an organ. Organs-on-chip models have been developed in order to create more reliable *in vitro* models compared to the commonly used static models, such as the Transwell setup. However, the BBB-on-chip models that exist today are still far from fully mimicking the very complex structure of the BBB and the NVU. As such, *in vivo* models are, and will continue to be, important models used for drug development and research. What the BBB-on-chip models can contribute with is more reliable early stage tests prior to *in vivo* tests, which would hopefully decrease the unnecessary use and suffering of animals.

# 8 Conclusion and recommendations

In this study the aim was to evaluate the influence on astrocytes and their culture environment on BBB modeling in a microfluidic chip. The project was divided into three experiments: culture astrocytes in different hydrogel compositions and evaluate the influence on the cells, incorporate a stable hydrogel in a microfluidic chip and in the final experiment establish a co-culture system with endothelial cells and astrocytes and measure the influence of astrocytes in the barrier integrity.

Astrocytes were cultured in different hydrogels and the results from this study indicate that there are significant differences in reactivity between astrocytes, although the results seem to correlate more with gel stiffness then the addition of HA. Hydrogels containing astrocytes distributed throughout the height of the gel were successfully incorporated in microfluidic channels with high attachment to channel walls. In the final experiment where the effects of a co-culture system were to be evaluated, there was no formation of a barrier due to decreased viability of the endothelial cells. The hydrogels that were incorporated in the chip failed after a few days in the chip with a varying viability of astrocytes inside the gels. These results indicate that the current chip design may not be suitable for the co-culture system applied in this study.

## 8.1 Future recommendations

The prospects of a co-culture system in a microfluidic chip are promising, however there are a few things that should be considered before implementing one.

First of all the incorporation of a hydrogel in the chip design used for these experiments should be optimized. Due to material properties of the chip the surface needs to be treated before interactions are achieved that are strong enough to maintain the structure of the hydrogel. Another complication with the current design is the incorporation of air bubbles in the chips, most likely due to the electrode compartment. If good solutions are found to address these two problems the current chip design can be used. However, another idea is to alter the chip design. If a suitable design is found this may be a better idea in order to decrease the risk of gel failure in the chip. One strong suggestion is to incorporate a medium channel, both to decrease the forces applied to the gel, but also to decrease the time of flushing the chip.

One of the main focuses in this report is the effect of culturing environment on astrocytes. From literature there are strong suggestions that the culture conditions have an important influence on astrocyte reactivity and morphology, especially comparing 2D and 3D cultures. The reactive state of astrocytes is reported to decrease the BBB integrity, it is important to evaluate the reactivity of the astrocytes used for BBB modeling. The commonly used astrocyte marker, GFAP, is upregulated during the reactive state of astrocytes making the evaluation of reactivity relatively easy to include in the evaluation of the model.

To measure GFAP expression the cells are often stained with antibodies and the intensity evaluated through image analysis. In order to ensure proper staining of the astrocytes and to avoid background noise that may limit the detection of lower expression levels, an optimization of the staining protocol should be performed. The recommendation is to test different dilutions of the staining in the system to be used. Especially when working with hydrogels the staining and washing steps will need different incubation times depending on the flushing method and the thickness of the gel. Another thing to consider is the use of a blocking buffer specific for the antibodies applied. For evaluation of intensity levels a suitable image analysis method for the system should be established. Since a high number of cells should be analyzed in order to get statistically relevant results the method should preferably be carried out automatically. Some problems that needs to addressed for a successful method is the handling of out-of-plane cells and background noise. If possible, 3D imaging with a confocal microscope should be considered.

The final recommendation is about the co-culturing of endothelial cells and astrocytes. There are several reports of increased barrier tightness after addition of astrocytes to the barrier. However, it is important to be aware that the influence varies between cell lines. Especially for hCMEC/D3, which is the cell line used in this study, the influence of astrocytes on the barrier tightness is reported to not be very large, although an increase has been reported. It is important to not only evaluate if astrocytes will increase the barrier tightness, but also to evaluate the effect of reactive astrocytes on the barrier physiology. There are a few studies where agents are added to increase the reactivity of astrocytes while measuring the effect on the barrier through TEER measurements. Nevertheless, due to the differences between cell lines further investigation of this is needed.

# References


[1] N. J. Abbott, L. Rönnbäck, and E. Hansson, "Astrocyte–endothelial interactions at the blood–brain barrier," *Nat. Rev. Neurosci.*, vol. 7, no. 1, pp. 41–53, 2006.

[2] A. Wolff, M. Antfolk, B. Brodin, and M. Tenje, "In Vitro Blood-Brain Barrier Models - An Overview of Established Models and New Microfluidic Approaches," *J. Pharm. Sci.*, vol. 104, no. 9, pp. 2727–2746, 2015.

[3] T. Ruck, S. Bittner, and S. Meuth, "Blood-brain barrier modeling: challenges and perspectives," *Neural Regen. Res.*, vol. 10, no. 6, p. 889, 2015.

[4] D. Huh, G. A. Hamilton, and D. E. Ingber, "From 3D cell culture to organs-on-chips," *Trends Cell Biol.*, vol. 21, no. 12, pp. 745–754, 2011.

[5] H. Cho *et al.*, "Three-Dimensional Blood-Brain Barrier Model for in vitro Studies of Neurovascular Pathology.," *Sci. Rep.*, vol. 5, p. 15222, 2015.

[6] K. L. Sellgren, B. T. Hawkins, and S. Grego, "An optically transparent membrane supports shear stress studies in a three-dimensional microfluidic neurovascular unit model," *Biomicrofluidics*, vol. 9, no. 6, pp. 1–4, 2015.

[7] R. Booth and H. Kim, "Characterization of a microfluidic in vitro model of the blood-brain barrier (μBBB)," *Lab Chip*, vol. 12, no. 10, p. 1784, 2012.

[8] M. W. van der Helm, A. D. van der Meer, J. C. T. Eijkel, A. van den Berg, and L. I. Segerink, "Microfluidic organ-on-chip technology for blood-brain barrier research.," *Tissue barriers*, vol. 4, no. 1, p. e1142493, 2016.

[9] G. Adriani *et al.*, "A 3D neurovascular microfluidic model consisting of neurons, astrocytes and cerebral endothelial cells as a blood–brain barrier," *Lab Chip*, vol. 12, pp. 169–182, 2017.

[10] A. Herland, A. D. Van Der Meer, E. A. FitzGerald, T. E. Park, J. J. F. Sleeboom, and D. E. Ingber, "Distinct contributions of astrocytes and pericytes to neuroinflammation identified in a 3D human blood-brain barrier on a chip," *PLoS One*, vol. 11, no. 3, pp. 1–21, 2016.

[11] N. J. Abbott, "Astrocyte-endothelial interactions and blood-brain barrier permeability," *J. Anat.*, vol. 200, no. 6, pp. 629–638, 2002.

[12] B. T. Hawkins, S. Grego, and K. L. Sellgren, "Three-dimensional culture conditions differentially affect astrocyte modulation of brain endothelial barrier function in response to transforming growth factor β1," *Brain Res.*, vol. 1608, pp. 167–176, 2015.

[13] B. T. Hawkins and T. P. Davis, "The Blood-Brain Barrier / Neurovascular Unit in Health and Disease," *Pharmacol. Rev.*, vol. 57, no. 2, pp. 173–185, 2005.

[14] N. J. Abbott, A. A. K. Patabendige, D. E. M. Dolman, S. R. Yusof, and D. J.

Begley, “Structure and function of the blood-brain barrier,” *Neurobiol. Dis.*, vol. 37, no. 1, pp. 13–25, 2010.

[15] F. L. Cardoso, D. Brites, and M. A. Brito, “Looking at the blood-brain barrier: Molecular anatomy and possible investigation approaches,” *Brain Res. Rev.*, vol. 64, no. 2, pp. 328–363, 2010.

[16] P. Naik and L. Cucullo, “In vitro blood-brain barrier models: Current and perspective technologies,” *J. Pharm. Sci.*, vol. 101, no. 4, pp. 1337–1354, 2012.

[17] S. N. Bhatia and D. E. Ingber, “Microfluidic organs-on-chips,” *Nat. Biotechnol.*, vol. 32, no. 8, pp. 760–772, 2014.

[18] I. Wilhelm, C. Fazakas, and I. A. Krizbai, “In vitro models of the blood-brain barrier,” *Acta Neurobiol Exp*, vol. 71, no. 1, pp. 113–128, 2011.

[19] E. A. Neuwelt *et al.*, “Engaging Neuroscience to Advance Translational Research in Brain Barrier Biology,” *Nat. Rev. Neurosci.*, vol. 12, no. 3, pp. 169–182, 2011.

[20] J. Banerjee, Y. Shi, and H. S. Azevedo, “In vitro blood–brain barrier models for drug research: state-of-the-art and new perspectives on reconstituting these models on artificial basement membrane platforms,” *Drug Discov. Today*, vol. 21, no. 9, pp. 1367–1386, 2016.

[21] B. D. B. Cines *et al.*, “Endothelial Cells in Physiology and in the Pathophysiology of Vascular Disorders,” *J. Am. Soc. Hematol.*, vol. 91, no. 10, pp. 3527–3561, 1998.

[22] J. Bicker, G. Alves, A. Fortuna, and A. Falcão, “Blood-brain barrier models and their relevance for a successful development of CNS drug delivery systems: A review,” *Eur. J. Pharm. Biopharm.*, vol. 87, no. 3, pp. 409–432, 2014.

[23] H. Wolburg and A. Lippoldt, “Tight junctions of the blood-brain barrier: Development, composition and regulation,” *Vascul. Pharmacol.*, vol. 38, no. 6, pp. 323–337, 2002.

[24] M. Saitou *et al.*, “Complex phenotype of mice lacking occludin, a component of tight junction strands.,” *Mol. Biol. Cell*, vol. 11, no. 12, pp. 4131–42, 2000.

[25] T. Nitta *et al.*, “Size-selective loosening of the blood-brain barrier in claudin-5-deficient mice,” *J. Cell Biol.*, vol. 161, no. 3, pp. 653–660, 2003.

[26] S. Chen, R. Einspanier, and J. Schoen, “Transepithelial electrical resistance (TEER): a functional parameter to monitor the quality of oviduct epithelial cells cultured on filter supports,” *Histochem. Cell Biol.*, vol. 144, no. 5, pp. 509–515, 2015.

[27] V. S. LeBleu, B. Macdonald, and R. Kalluri, “Structure and function of basement membranes.,” *Exp. Biol. Med. (Maywood).*, vol. 232, no. 9, pp. 1121–9, 2007.

[28] K. M. Baeten and K. Akassoglou, “Extracellular Matrix and Matrix Receptors in

Blood-Brain Barrier Formation and Stroke," *Dev Neurobiol.*, vol. 71, no. 11, pp. 1018–1039, 2011.

[29] A. Trost *et al.*, "Brain and Retinal Pericytes: Origin, Function and Role.," *Front. Cell. Neurosci.*, vol. 10, no. February, p. 20, 2016.

[30] M. V. Sofroniew and H. V. Vinters, "Astrocytes: Biology and pathology," *Acta Neuropathol.*, vol. 119, no. 1, pp. 7–35, 2010.

[31] J. L. Ridet, S. K. Malhotra, A. Privat, and F. H. Gage, "Reactive astrocytes: Cellular and molecular cues to biological function," *Trends Neurosci.*, vol. 20, no. 12, pp. 570–577, 1997.

[32] L. F. Eng, "Glial fibrillary acidic protein (GFAP): the major protein of glial intermediate filaments in differentiated astrocytes," *J. Neuroimmunol.*, vol. 8, no. C, pp. 203–214, 1985.

[33] Y. K. Choi and K.-W. Kim, "Blood-neural barrier: its diversity and coordinated cell-to-cell communication.," *BMB Rep.*, vol. 41, no. 5, pp. 345–52, 2008.

[34] D. Attwell, A. Buchan, S. Charpak, M. Lauritzen, B. MacVicar, and E. Newman, "Glial and neuronal control of brain blood flow," *Nature*, vol. 468, no. 7321, pp. 232–243, 2011.

[35] B. V. Zlokovic, "The Blood-Brain Barrier in Health and Chronic Neurodegenerative Disorders," *Neuron*, vol. 57, no. 2, pp. 178–201, 2008.

[36] M. E. Lull and M. L. Block, "Microglial activation and chronic neurodegeneration.," *Neurotherapeutics*, vol. 7, no. 4, pp. 354–65, 2010.

[37] A. C. da Fonseca *et al.*, "The impact of microglial activation on blood-brain barrier in brain diseases," vol. 8, no. November, pp. 1–13, 2014.

[38] D. R. Zimmermann and M. T. Dours-Zimmermann, "Extracellular matrix of the central nervous system: From neglect to challenge," *Histochem. Cell Biol.*, vol. 130, no. 4, pp. 635–653, 2008.

[39] D. Bonneh- Barkay and C. Wiley, "Brain extracellular matrix in neurodegeneration," *Brain Pathol.*, vol. 19, no. 4, pp. 573–585, 2009.

[40] C. Nicholson, "Diffusion and related transport mechanisms in brain tissue," *Reports Prog. Phys.*, vol. 64, no. 7, pp. 815–884, 2001.

[41] H. Xu *et al.*, "A dynamic in vivo-like organotypic blood-brain barrier model to probe metastatic brain tumors," *Sci. Rep.*, vol. 6, no. November, p. 36670, 2016.

[42] P. Pound and M. B. Bracken, "Is animal research sufficiently evidence based to be a cornerstone of biomedical research?," *Bmj*, vol. 348, no. may30 1, pp. g3387–g3387, 2014.

[43] S. Perrin, "Preclinical research: Make mouse studies work," *Nature*, vol. 507, no.

7493, pp. 423–425, 2014.

[44] A. R. Perestrelo, A. C. P. Águas, A. Rainer, and G. Forte, “Microfluidic organ/body-on-a-chip devices at the convergence of biology and microengineering,” *Sensors (Switzerland)*, vol. 15, no. 12, pp. 31142–31170, 2015.

[45] A. D. Wong, M. Ye, A. F. Levy, J. D. Rothstein, D. E. Bergles, and P. C. Searson, “The blood-brain barrier: an engineering perspective,” *Front. Neuroeng.*, vol. 6, no. August, pp. 1–22, 2013.

[46] K. Hatherell, P. O. Couraud, I. A. Romero, B. Weksler, and G. J. Pilkington, “Development of a three-dimensional, all-human in vitro model of the blood-brain barrier using mono-, co-, and tri-cultivation Transwell models,” *J. Neurosci. Methods*, vol. 199, no. 2, pp. 223–229, 2011.

[47] G. Li *et al.*, “Permeability of endothelial and astrocyte cocultures: In vitro Blood-brain barrier models for drug delivery studies,” *Ann. Biomed. Eng.*, vol. 38, no. 8, pp. 2499–2511, 2010.

[48] C. R. White and J. A. Frangos, “The shear stress of it all: the cell membrane and mechanochemical transduction,” *Philos. Trans. R. Soc. B Biol. Sci.*, vol. 362, no. 1484, pp. 1459–1467, 2007.

[49] H. C. Helms *et al.*, “In vitro models of the blood–brain barrier: An overview of commonly used brain endothelial cell culture models and guidelines for their use,” *J. Cereb. Blood Flow Metab.*, vol. 36, no. 5, pp. 862–890, 2016.

[50] D. Huh, Y. Torisawa, G. A. Hamilton, H. J. Kim, and D. E. Ingber, “Microengineered physiological biomimicry: Organs-on-Chips,” *Lab Chip*, vol. 12, no. 12, p. 2156, 2012.

[51] D. Huh, B. D. Matthews, A. Mammoto, H. Y. Hsin, and D. E. Ingber, “Reconstituting Organ-Level Lung Functions on a Chip,” *Science (80-. ).*, vol. 328, pp. 1662–1668, 2010.

[52] S. Hyun, J. Kim, and D. E. Ingber, “Gut-on-a-Chip microenvironment induces human intestinal cells to undergo villus differentiation,” *Integr. Biol.*, vol. 5, no. 207890, pp. 1130–1140, 2013.

[53] L. M. Griep *et al.*, “BBB on CHIP: Microfluidic platform to mechanically and biochemically modulate blood-brain barrier function,” *Biomed. Microdevices*, vol. 15, no. 1, pp. 145–150, 2013.

[54] B. Srinivasan, A. R. Kolli, M. B. Esch, H. E. Abaci, M. L. Shuler, and J. J. Hickman, “TEER Measurement Techniques for In Vitro Barrier Model Systems.,” *J. Lab. Autom.*, vol. 20, no. 2, pp. 107–126, 2015.

[55] S. M. Stamatovic, R. F. Keep, and A. V Andjelkovic, “Brain endothelial cell-cell junctions: how to ‘open’ the blood brain barrier.,” *Curr. Neuropharmacol.*, vol. 6, no. 3, pp. 179–92, 2008.

[56] J. Haorah, K. Schall, S. H. Ramirez, and Y. Persidsky, “Activation of protein tyrosine kinases and matrix metalloproteinases causes blood-brain barrier injury: Novel mechanism for neurodegeneration associated with alcohol abuse,” *Glia*, vol. 56, no. 1, pp. 78–88, 2008.

[57] K. Benson, S. Cramer, and H.-J. Galla, “Impedance-based cell monitoring: barrier properties and beyond,” *Fluids Barriers CNS*, vol. 10, no. 1, p. 5, 2013.

[58] N. J. Douville, Y. C. Tung, R. Li, J. D. Wang, M. E. H. El-Sayed, and S. Takayama, “Fabrication of two-layered channel system with embedded electrodes to measure resistance across epithelial and endothelial barriers,” *Anal. Chem.*, vol. 82, no. 6, pp. 2505–2511, 2010.

[59] C. Lohmann, S. Hüwel, and H.-J. Galla, “Predicting Blood-Brain Barrier Permeability of Drugs: Evaluation of Different In Vitro Assays,” *J. Drug Target.*, vol. 10, no. 4, pp. 263–276, 2002.

[60] A. Hoffmann, J. Bredno, M. Wendland, N. Derugin, P. Ohara, and M. Wintermark, “High and Low Molecular Weight Fluorescein Isothiocyanate (FITC)-Dextrans to Assess Blood-Brain Barrier Disruption: Technical Considerations,” *Transl. Stroke Res.*, vol. 2, no. 1, pp. 106–111, 2011.

[61] M. W. van der Helm *et al.*, “Direct quantification of transendothelial electrical resistance in organs-on-chips,” *Biosens. Bioelectron.*, vol. 85, pp. 924–929, 2016.

[62] J. H. Yeon, D. Na, K. Choi, S. W. Ryu, C. Choi, and J. K. Park, “Reliable permeability assay system in a microfluidic device mimicking cerebral vasculatures,” *Biomed. Microdevices*, vol. 14, no. 6, pp. 1141–1148, 2012.

[63] A. Mata, A. J. Fleischman, and S. Roy, “Characterization of polydimethylsiloxane (PDMS) properties for biomedical micro/nanosystems.,” *Biomed. Microdevices*, vol. 7, no. 4, pp. 281–293, 2005.

[64] C. Cha *et al.*, “Tailoring hydrogel adhesion to polydimethylsiloxane substrates using polysaccharide glue,” *Angew. Chemie - Int. Ed.*, vol. 52, no. 27, pp. 6949–6952, 2013.

[65] D. Bodas and C. Khan-Malek, “Hydrophilization and hydrophobic recovery of PDMS by oxygen plasma and chemical treatment-An SEM investigation,” *Sensors Actuators, B Chem.*, vol. 123, no. 1, pp. 368–373, 2007.

[66] T. Trantidou, Y. Elani, E. Parsons, and O. Ces, “Hydrophilic surface modification of PDMS for droplet microfluidics using a simple, quick, and robust method via PVA deposition,” *Microsystems Nanoeng.*, vol. 3, no. November 2016, p. 16091, 2017.

[67] K. M. Kovach, J. R. Capadona, A. Sen Gupta, and J. A. Potkay, “The effects of PEG-based surface modification of PDMS microchannels on long-term hemocompatibility,” *J. Biomed. Mater. Res. - Part A*, vol. 102, no. 12, pp. 4195–4205, 2014.

[68] A. Siddique, T. Meckel, R. W. Stark, and S. Narayan, “Improved cell adhesion under shear stress in PDMS microfluidic devices,” *Colloids Surfaces B Biointerfaces*, vol. 150, pp. 456–464, 2017.

[69] I. Wong and C.-M. Ho, “Surface molecular property modifications for poly(dimethylsiloxane) (PDMS) based microfluidic devices,” *Microfluid Nanoflui*, vol. 7, pp. 291–306, 2009.

[70] S. Kuddannaya and Y. Chuah, “Surface chemical modification of poly (dimethylsiloxane) for the enhanced adhesion and proliferation of mesenchymal stem cells,” *ACS Appl. Mater. Interfaces*, vol. 5, pp. 9777–9784, 2013.

[71] R. Edmondson, J. J. Broglie, A. F. Adcock, and L. Yang, “Three-Dimensional Cell Culture Systems and Their Applications in Drug Discovery and Cell-Based Biosensors,” *Assay Drug Dev. Technol.*, vol. 12, no. 4, pp. 207–218, 2014.

[72] M. W. Tibbitt and K. S. Anseth, “Hydrogels as extracellular matrix mimics for 3D cell culture,” *Biotechnol. Bioeng.*, vol. 103, no. 4, pp. 655–663, 2009.

[73] J. Zhu and R. E. Marchant, “Design properties of hydrogel tissue-engineering scaffolds,” *Expert Rev. Med. Devices*, vol. 8, no. 5, pp. 607–626, 2011.

[74] K. Y. Lee and D. J. Mooney, “Hydrogels for tissue engineering,” *Chem. Rev.*, vol. 101, no. 7, pp. 1869–1879, 2001.

[75] M. D. Shoulders and R. T. Raines, “Collagen structure and stability,” *Annu Rev Biochem.*, vol. 78, pp. 929–958, 2009.

[76] N. C. Hunt and L. M. Grover, “Cell encapsulation using biopolymer gels for regenerative medicine,” *Biotechnol. Lett.*, vol. 32, no. 6, pp. 733–742, 2010.

[77] A. L. Placone, P. M. McGuiggan, D. E. Bergles, H. Guerrero-Cazares, A. Quiñones-Hinojosa, and P. C. Searson, “Human astrocytes develop physiological morphology and remain quiescent in a novel 3D matrix,” *Biomaterials*, vol. 42, pp. 134–143, 2015.

[78] M. Verhulsel, M. Vignes, S. Descroix, L. Malaquin, D. M. Vignjevic, and J. L. Viovy, “A review of microfabrication and hydrogel engineering for micro-organs on chips,” *Biomaterials*, vol. 35, no. 6, pp. 1816–1832, 2014.

[79] G. Kogan, L. Šoltés, R. Stern, and P. Gemeiner, “Hyaluronic acid: A natural biopolymer with a broad range of biomedical and industrial applications,” *Biotechnol. Lett.*, vol. 29, no. 1, pp. 17–25, 2007.

[80] J. A. Burdick and G. D. Prestwich, “Hyaluronic acid hydrogels for biomedical applications,” *Adv. Mater.*, vol. 23, no. 12, pp. 41–56, 2011.

[81] S. K. Seidlits *et al.*, “The effects of hyaluronic acid hydrogels with tunable mechanical properties on neural progenitor cell differentiation,” *Biomaterials*, vol. 31, no. 14, pp. 3930–3940, 2010.

[82] B. B. Weksler *et al.*, “Blood-brain barrier-specific properties of a human adult brain endothelial cell line.,” *FASEB J.*, vol. 19, no. 13, pp. 1872–1874, 2005.

[83] S. Schildge, C. Bohrer, K. Beck, and C. Schachtrup, “Isolation and culture of mouse cortical astrocytes.,” *J. Vis. Exp.*, no. 71, p. e50079, 2013.

[84] C. Pan, C. Kumar, S. Bohl, U. Klingmueller, and M. Mann, “Comparative proteomic phenotyping of cell lines and primary cells to assess preservation of cell type-specific functions.,” *Mol. Cell. Proteomics*, vol. 8, no. 3, pp. 443–450, 2009.

[85] X. Hu, V. Laguerre, D. Packert, A. Nakasone, and L. Moscinski, “A Simple and efficient method for preparing cell slides and staining without using cytocentrifuge and cytoclips,” *Int. J. Cell Biol.*, vol. 2015, 2015.

[86] J. A. Ramos-Vara, “Technical aspects of immunohistochemistry.,” *Vet. Pathol.*, vol. 42, no. 4, pp. 405–426, 2005.

[87] M. W. van der Helm, “Blood-brain barrier on a microfluidic chip,” *Univ. Twente*, vol. Master the, 2014.

[88] J. W. Park, B. Vahidi, A. M. Taylor, S. W. Rhee, and N. L. Jeon, “Microfluidic culture platform for neuroscience research.,” *Nat. Protoc.*, vol. 1, no. 4, pp. 2128–36, 2006.

[89] Y. J. Chuah, S. Kuddannaya, M. H. A. Lee, Y. Zhang, and Y. Kang, “The effects of poly(dimethylsiloxane) surface silanization on the mesenchymal stem cell fate,” *Biomater. Sci.*, vol. 3, no. 2, pp. 383–390, 2015.

[90] Y. Shin *et al.*, “Microfluidic assay for simultaneous culture of multiple cell types on surfaces or within hydrogels.,” *Nat. Protoc.*, vol. 7, no. 7, pp. 1247–59, 2012.

[91] W. Tan and T. A. Desai, “Microfluidic Patterning of Cellular Biopolymer Matrices for Biomimetic 3-D Structures,” *Biomed. Microdevices*, vol. 5, pp. 235–244, 2003.

[92] P. P. Partyka *et al.*, “Mechanical stress regulates transport in a compliant 3D model of the blood-brain barrier,” *Biomaterials*, vol. 115, pp. 30–39, 2017.

[93] N. A. Oberheim, S. A. Goldman, and M. Nedergaard, “Heterogeneity of Astrocytic Form and Function,” *Methods Mol Biol.*, vol. 814, pp. 23–45, 2012.

[94] D. R. Goddard, M. Berry, S. L. Kirvell, and A. M. Butt, “Fibroblast growth factor-2 induces astroglial and microglial reactivity in vivo,” *J. Anat.*, vol. 200, no. 1, pp. 57–67, 2002.

[95] C. A. McKay *et al.*, “An injectable, calcium responsive composite hydrogel for the treatment of acute spinal cord injury,” *ACS Appl. Mater. Interfaces*, vol. 6, no. 3, pp. 1424–1438, 2014.

[96] K. J. K. Regehr *et al.*, “Biological implications of polydimethylsiloxane-based

microfluidic cell culture," *Lab Chip*, vol. 9, no. 15, pp. 2132–2139, 2009.

[97] A. Cowley and B. Woodward, "A healthy future: Platinum in medical applications platinum group metals enhance the quality of life of the global population," *Platin. Met. Rev.*, vol. 55, no. 2, pp. 98–107, 2011.

[98] R. Li *et al.*, "A Rapidly Fabricated Microfluidic Chip for Cell Culture," *J. Chromatogr. Sci.*, vol. 54, no. 4, pp. 523–530, 2016.

[99] K. Zeng and D. Zhang, "Recent progress in alkaline water electrolysis for hydrogen production and applications," *Prog. Energy Combust. Sci.*, vol. 36, no. 3, pp. 307–326, 2010.

[100] E. East, J. P. Golding, and J. B. Phillips, "A versatile 3D culture model facilitates monitoring of astrocytes undergoing reactive gliosis," *J. Tissue Eng. Regen. Med.*, vol. 3, no. 7, pp. 634–646, 2009.

[101] V. Vickerman, J. Blundo, S. Chung, and R. D. Kamm, "Design, fabrication and implementation of a novel multi-parameter control microfluidic platform for three-dimensional cell culture and real-time imaging," *Lab Chip*, vol. 8, no. 9, pp. 1468–1477, 2008.

[102] L. S. Payne and P. H. Huang, "The pathobiology of collagens in glioma," *Mol. Cancer Res.*, vol. 11, no. 10, pp. 1–21, 2013.

[103] C. M. Lin *et al.*, "Hyaluronic acid inhibits the glial scar formation after brain damage with tissue loss in rats," *Surg. Neurol.*, vol. 72, no. SUPPL. 2, pp. S50–S54, 2009.

[104] B. Weksler, I. A. Romero, and P.-O. Couraud, "The hCMEC/D3 cell line as a model of the human blood brain barrier," *Fluids Barriers CNS*, vol. 10, no. 1, p. 16, 2013.

[105] R. Cabezas *et al.*, "Astrocytic modulation of blood brain barrier: perspectives on Parkinson's disease," *Front. Cell. Neurosci.*, vol. 8, no. August, pp. 1–11, 2014.

# Appendix

## A. Protocols

### *Chip fabrication*

PDMS base agent was mixed with the curing agent at a 10:1 wt ratio (Sylgard 184 Silicone elastomer kit, Dow Corning). The mix was degassed in vacuum for 1.5 h to remove air bubbles. A wafer with the desired chip design (prepared with a SU-8 mold fabrication process) was cleaned with an air blow gun and covered with PDMS, degassed for another 30 min and then baked in the oven at 60°C for at least 4 hours. When done baking, the PDMS mold was carefully removed from the wafer and cut into chips using a razorblade. The holes accessing the channels were made in the top parts of the chips with a 1 mm biopsy punch (Integra Miltex). In order to keep the chips clean they were covered with Scotch tape (3M). For the experiments two different chip designs were used and in the following sections the assembly of these chips will be described in further detail.

A single-channel PDMS chip with one inlet and one outlet was bonded to a glass cover slip coated with PDMS. Prior to bonding of the chip to a glass cover slip (24mm · 40 mm, Knittel Glass) the glass cover slip was coated with a thin layer of PDMS by adding 200 µl of PDMS and spin-coating it for 180 s at 6000 rpm (Spin 150, Polos, the Netherlands). The PDMS was made the same way as for the chips and degassed prior to use. The glass cover slips covered with PDMS were baked in the oven at 60°C for at least 2 h and then the chips and the glass slides were treated with oxygen plasma (Cute, Femto Science). Directly after the plasma treatment chip and glass cover slips were bonded and left in room temperature for at least 24 h.

A two-compartment PDMS chip contains two channels aligned perpendicular to each other with four inlets and outlets. In connection to each channel there are two electrode channels and a polycarbonate membrane separates the two channels. To connect the top part with the bottom part a glue was used made of PDMS and curing agent with a 10:1 wt ratio, mixed together with toluene (Merck) at a 5:3 wt ratio. Glue was applied to a glass cover slip and spin coated for 60 seconds at 1500 rpm. The glue was applied to the chip parts and a polycarbonate membrane (Transwell culture inserts, Corning Incorporated) was positioned over the middle of the channel prior to the alignment of the parts. As a last step the chips were baked in 60°C for 3 h [61].

*Cell culturing*

For the culturing of astrocytes, primary human astrocytes were used (ScienCell Research Laboratories). They were grown in T75 flasks, either pre-coated with PLL (Sigma Aldrich) or without pre-coating (Cellstar). For the experiments cells at passage number of 4-9 were used. The cells were grown in astrocyte medium (AM: Gibco) and when passaged the cells were washed with PBS (Sigma), detached from the flask with 0.05% trypsin-EDTA (Gibco) and after 5 min of incubation at 37°C in humidified air containing 5% $CO_2$, RPMI+ (RPMI medium, fetal bovine serum (10% of the total volume), Penicillin Streptomycin and L-glutamine; Gibco) was added to deactivate the trypsin-EDTA. The suspension was centrifuged at 390g for 5 min and the cell pellet was re-suspended in new medium. The cells were either subcultured in a new flask or used for experiments.

For brain endothelium, the hCMEC/D3 cell line was used for these experiments. They were grown in T75 flasks, pre-coated with fibronectin or collagen type I (Cellcoat). For the experiments in this report cells at a passage number of 34 and 35 were used and they were grown in EGM-2 (EBM-2 with EGM-2 SingleQuots, Lonza).

*Hydrogels*

In all experiments hydrogels were made at different concentrations and components. All the volumes added of each component for the three experiments have been summarized in Table 4.

**Table 4.** Table summarizing the concentrations and volumes used to make the hydrogels in the three experiments. In experiment three, four different tubes with the exact same volumes were made to decrease the risk of early gelling in the tube, and therefore the volumes used for only one tube is presented in the table. C- collagen type I and HA- hyaluronic acid.

| | Exp 1 | Exp 2 | Exp 2 | Exp 2 | Exp 2 | Exp 2 | Exp 3 |
|---|---|---|---|---|---|---|---|
| Condition | C 3 | C 4 | C:HA 3:1 | C:HA 4:1 | C:HA 5:1 | C:HA 4:2 | C:HA 3:1 |
| Collagen stock (mg/ml) | 9.66 | 8.56 | 8.56 | 8.56 | 8.56 | 8.56 | 8.56 |
| HA stock (mg/ml) | - | - | 10 | 10 | 10 | 10 | 10 |
| Total volume (µl) | 300 | 150 | 150 | 150 | 150 | 150 | 200 |
| 10 X PBS (µl) | 10 | 7.78 | 5.84 | 7.78 | 9.73 | 7.78 | 7.8 |
| 1 M NaOH (µl) | 2.1 | 1.6 | 1.2 | 1.6 | 2 | 1.6 | 1.6 |
| Collagen type I (µl) | 93 | 70 | 52.6 | 70 | 87.6 | 70 | 70 |
| HA (µl) | - | - | 15 | 15 | 15 | 30 | 20 |
| PEGDA (µl) | - | - | 3.75 | 3.75 | 3.75 | 7.5 | 5 |
| Cells in AM (µl) | 195 | 70.62 | 71.61 | 51.87 | 31.92 | 33.12 | 95.6 |

*Staining of cells*

Fixation of the cells was carried out by removing medium from the system by flushing twice with PBS. The flushing step was performed by leaving a pipette tip with 100 µl of PBS connected to the inlet for 30-60 min. If carried out in a wells plate the medium was removed by pipetting and PBS was added for 15 min. A 3.7-4% (para)formaldehyde solution was added in order to fixate the cells and the samples were incubated with the solution at room temperature for 30-60 min. Afterwards they were washed three times with PBS for 30-60 min and stored covered in PBS at 4°C until staining.

*Staining in 2D*

When staining with antibodies, the primary antibody was diluted in 0.1% (v/v) Triton-X 100 (Sigma Aldrich) and 1% (m/m) bovine serum albumin (BSA: Sigma Aldrich) in PBS and the fixated cells were incubated in the solution overnight at 4°C (rat anti-GFAP 1:50 (Invitrogen)). The cells were flushed with PBS three times and afterwards incubated with the diluted secondary antibody and additional stainings in Triton-X 0.01% + BSA for 1 hour (goat anti-rat IgG Alexa Flour 488 1:100 (Invitrogen); goat anti-rat IgG Alexa Flour 568 1:100 (Molecular probes, Life Technologies); NucBlue 2 drops/mL (Molecular Probes, Life Technologies); ActinGreen 2 drops/mL (Molecular Probes, Life Technologies); Texas Red-X Phalloidin 1:40 (Invitrogen)). In the final step the cells were washed three times with PBS.

*Staining in hydrogel*

When staining with antibodies, the primary antibody was diluted in 0.1% Triton-X and 1% BSA and the gels were incubated in the solution overnight at 4°C (rat anti-GFAP 1:50). The gels were flushed with PBS for at least 6 hours, changing the pipette tips (containing 100µl only added to the inlet) every hour. Afterwards, the samples were incubated with the diluted secondary antibody and additional stainings in 0.1% Triton-X and 1% BSA overnight at room temperature or 4°C (goat anti-rat IgG Alexa Flour 488 1:100; goat anti-rat IgG Alexa Flour 568 1:100; NucBlue 2 drops/mL; ActinGreen 2 drops/mL; Texas Red-X Phalloidin 1:40). In the final step the gels were flushed with PBS for at least 6 h, changing the pipette tips every hour.

*Microscopy*

For phase contrast imaging and fluorescence imaging the EVOS FL Cell Imaging System microscope was used (Life Technologies). Four fluorescent filter cubes were applied depending on staining; green (GFP) with excitation wavelength of 470/22 nm and emission wavelength of 525/50 nm, blue (DAPI) with an excitation wavelength of 357/44 nm and emission wavelength of 447/60 nm, red (RFP) with an excitation wavelength of 531/40 nm and emission wavelength of 593/40 nm and infra-red (CY5) with an excitation wavelength of 628/40 nm and emission wavelength of 685/40 nm (Life Technologies).

To obtain three dimensional images a Nikon Confocal A1 microscope was used. For the samples mentioned in this report excitation lasers with wavelengths of

405 nm for emission of blue light and 488 nm for emission of green light were used.

## B. Hydrogel composition in chips

*Materials and methods*

A total of 12 chips and two wells in a 96 wells plate were used for the experiment. A chip design with a PDMS chip containing a single channel attached to a PDMS covered glass cover slip was used (see appendix A. Chip fabrication). The surfaces of the channels were treated with APTES and GA prior to adding the gels (for protocol, see section 4.1).

Five different gel concentrations with varying collagen type I and HA concentrations were tested together with controls for the staining: astrocytes seeded in 2D for positive control and endothelial cells seeded in a hydrogel for negative control. All conditions are summarized in Table 5. Astrocytes at a passage number of 9 and endothelial cells at a passage number of 35 were used. A fixed cell concentration of $2.5 \cdot 10^5$ cells/ml was used for all the chips while hydrogel concentrations were varied.

**Table 5.** Table summarizing the 7 different conditions used in the experiment. In condition 1 astrocytes were seeded in a collagen type I gel was used as a positive control. In conditions 2-5 astrocytes were seeded in gels where the concentrations of collagen type I and HA were varied. Condition 6 has endothelial cells seeded in a collagen type I gel for negative control, and in the final condition astrocytes are cultured in 2D in wells plates. A – astrocytes, E – endothelial cells and W – wells plate.

| Condition | 1 | | 2 | | 3 | | 4 | | 5 | | 6 | | 7 | |
|---|---|---|---|---|---|---|---|---|---|---|---|---|---|---|
| Cell type | A | | A | | A | | A | | A | | E | | A | |
| Collagen concentration (mg/ml) | 4 | | 3 | | 4 | | 5 | | 4 | | 4 | | 0 | |
| HA concentration (mg/ml) | 0 | | 1 | | 1 | | 1 | | 2 | | 0 | | 0 | |
| Chip number | 1 | 2 | 3 | 4 | 5 | 6 | 7 | 8 | 9 | 10 | 11 | 12 | W | W |

All the gels were made according to the following protocol with varying volumes depending on the condition. 10X PBS, 1M NaOH and AM were added to Eppendorf tubes and put on ice. Afterwards, the collagen type I and HA mixed with poly(ethylene glycol) diacrylate (PEGDA; Glycosan HyStem Trial Kit) at a ratio of 1:4 was added, according to manufacturer's recommendations. In the final step the cells were detached from the culture flasks and resuspended in AM or EGM-2 and added to the Eppendorf tubes. After mixing of the liquid gel through pipetting, it was added to the chips. The gels were left to incubate at 37°C for 30

min in order to gel, before 100 µl of medium was added to the inlet of the channel, and an empty pipette tip to the outlet. In two wells of a 96 wells plate astrocytes were seeded at a concentration of $2.0 \cdot 10^4$ cells/cm$^2$.

Medium was refreshed twice per day during the 48 h that the experiment lasted for and time frames were taken of the cells after 4 h, 24 h and 48 h with phase contrast microscopy. After 48 h the cells were fixated and stained with ActinGreen, NucBlue, primary antibody rat anti-GFAP and secondary antibody goat anti-rat IgG Alexa Fluor 568 according to protocols in appendix A. Staining of cells, and imaged with fluorescent microscopy.

*Results and discussion*

In the experiment a total of 12 chips were filled with cells seeded in different hydrogel compositions. Furthermore, two wells in a 96 well plate were seeded with astrocytes directly on the bottom of the well. All chips were successfully filled, only in one chip an air bubble was incorporated close to the inlet which caused the flow in the chip to be blocked. In three chips the gel detached from the walls and these were not stained. In Table 6 the different conditions and the results from the chips prior to staining are shown.

**Table 6.** Summary of the conditions of the chips after the experiment was finished. S – staining, D – detached gel and X – damage to chip.

| Condition | 1 | | 2 | | 3 | | 4 | | 5 | | 6 | |
|---|---|---|---|---|---|---|---|---|---|---|---|---|
| Chip number | 1 | 2 | 3 | 4 | 5 | 6 | 7 | 8 | 9 | 10 | 11 | 12 |
| 48 h | S | S | D | S | S | S | D | S | X | S | S | D |

After the 48 h duration of the experiment the cells were stained and from the staining it was shown that the viability in the chips was very low. There were a few cells that had short and few processes and some expressed GFAP, as can be seen in Figure 40.

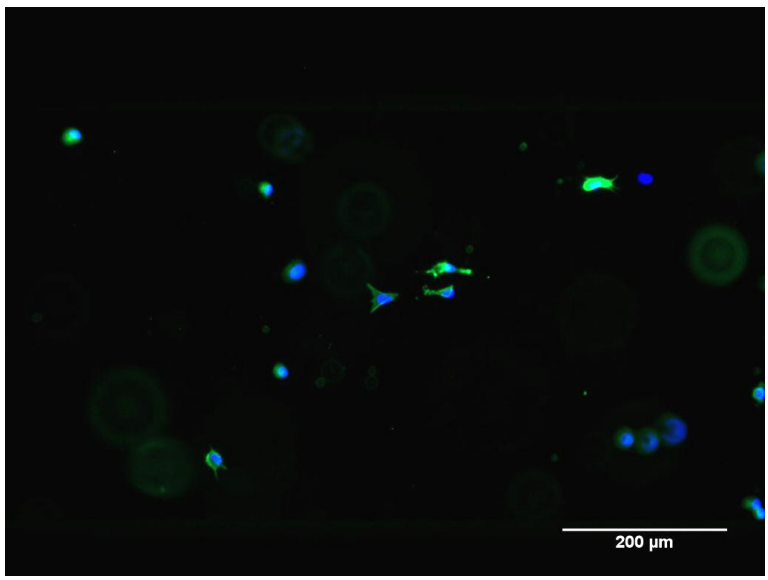


**Figure 40.** Image from chip 1 where few astrocytes with processes are visible. Image taken with fluorescent microscopy using GFP and DAPI filter. Scale bar is 200 µm.

From images taken at the three different time frames of 4, 24 and 48 h, see Figure 41-43, living cells with spread out processes are seen at 4 h, while at 48 h very few viable cells with the typical morphology are visible, implicating that the viability of the cells decreased after the cells had been added to the chips.

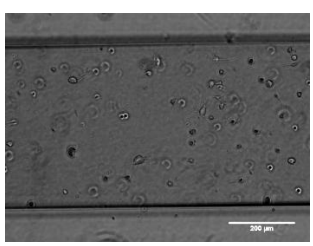

**Figure 41.** Image of the channel in chip 10, 4 h after the gel had been added. Viable cells with spread out processes are visible. Taken with phase contrast microscopy and scale bar is 200 µm.

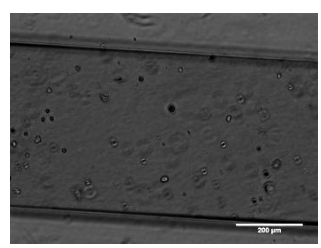

**Figure 42.** Image of the channel in chip 10, 24 h after the gel had been added. Few viable cells with spread out processes are visible. Taken with phase contrast microscopy and scale bar is 200 µm.

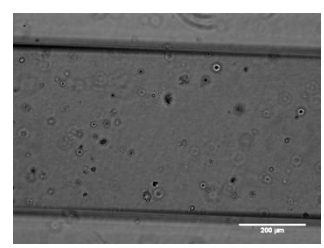

**Figure 43.** Image of the channel in chip 10, 48 h after the gel had been added. Barely any viable cells with spread out processes are visible. Taken with phase contrast microscopy and scale bar is 200 µm.

A cause for the decreased viability in the chip was first hypothesized to be nutrition deficiency. However, after some further consideration another suggestion was that the low cell concentration together with a high medium flow could be the cause for the decreased viability. The difference in this experiment in comparison to the one with surface treatment was that the cell concentration was

lowered and the method of changing medium was changed. In the prior experiment a pipette tip with 150 µl was inserted in the inlet and 100 µl in the outlet, while in this experiment the medium was changed by a pipette tip with 100 µl in the inlet and an empty pipette tip in the outlet. A higher flow will mean that the cells will be exposed to higher forces. There is also a risk that the flow flushes away signaling molecules that due to the low cell concentration are present in low concentrations. This unfamiliar environment for the astrocytes may cause the decreased viability. However, to confirm this hypothesis further investigation is needed.